Rheological controls on the eruption potential and style of an andesite volcano: a case study from Mt. Ruapehu, New Zealand

G.N. Kilgour[1,2,*], H.M.Mader[1], J.D. Blundy[1], R.A. Brooker[1]

[1] *School of Earth Sciences, University of Bristol, Wills Memorial Building, Queens Road, Bristol, BS8 1RJ, UK*

[2] *GNS Science, Wairakei Research Centre, Private Bag 2000, Taupo, New Zealand*

[*] *Corresponding author*

g.kilgour@gns.cri.nz

Tel.: +64 7 3748211

Abstract

The evolving magma rheology of three recent Ruapehu eruptions (1969, 1977, and 1995) is estimated using a combination of thermodynamic models and rheological calculations, supported by textural observations of the erupted scoria. We use a well-established thermodynamic model to determine the composition of these representative Ruapehu magmas from 300 MPa to $\sim$ 30 MPa. The outputs of the model provide the changing crystal and bubble content in a closed system (assuming no gas loss), as well as the fractionating melt compositions. We calculate the melt viscosity, and the effect of bubbles and crystals, to quantify the rheology of the magma during ascent (under assumed equilibrium conditions). The moderately high phenocryst content of Ruapehu scoria ($\sim$ 30 %) means that only a small amount of additional microlite crystallisation ($\sim$ 5 %) would result in a yield strength, which may lead the magma to stall. However, if the strain rates are high enough, more crystallisation would be possible without developing a yield stress. This suggests that microlite-rich magmas are almost certain to stall unless they encounter significant fluid addition from a source such as a hydrothermal system, groundwater, or surface water (i.e., Ruapehu's Crater Lake).

Ruapehu magmas are initially H_2O-undersaturated and as a consequence, crystallisation and bubble growth were suppressed until the magma achieved saturation, at $\sim$ 100 to 50 MPa. From this analysis, we suggest that Ruapehu magmas are more likely to erupt compared to magmas of a similar composition that are H_2O-saturated. This partly explains the regular, albeit small-volume eruptions at Ruapehu and the propensity for phreatomagmatic eruptions when the magma:water ratio is low.

1. Introduction

The physical state of a magma controls a range of igneous processes, including crystal and bubble growth (e.g., Llewellin et al., 2002b; Hammer, 2008), the ability to exsolve gas (e.g., Gonnermann and Manga, 2007), or drive convection (e.g., Huppert and Sparks, 1981), and eventually whether the magma erupts or stalls (e.g., Caricchi et al., 2008). During magma ascent, crystallisation and bubble expansion significantly alter the physical properties of a magma. Therefore, a quantitative assessment of magma rheology through time could help to explain the style, duration and size of eruptions. The aim of this work is to develop a method for determining the rheology of magma from storage to eruption using existing constitutive equations. An assessment of the changing rheological properties of magma could provide insights into the generation of seismicity, deformation, and gas efflux; all signals that are regularly monitored at active volcanoes.

Early research into the physical properties of magma were restricted to the liquid phase. Bottinga and Weill (1970, 1972) and Shaw (1972) were the first to describe melt viscosity and density as a function of temperature and composition. More recent work used high temperature (and sometimes pressure) experiments to develop a more robust, universal viscosity equation that fully considers the effect of H_2O and F on melt viscosity (Giordano and Dingwell, 2003; Giordano et al., 2004; Hui and Zhang, 2007; Giordano et al., 2008). The formulation of Giordano et al. (2008) is currently well accepted and will be used throughout.

The addition of crystals to a melt has been experimentally examined at high temperature and pressure on natural or synthetic suspensions (e.g., Lejeune and Richet, 1995; Sato, 2005; Ishibashi and Sato, 2007; Lavallee et al., 2007; Caricchi et al., 2008; Cordonnier et al., 2009; Ishibashi, 2009; Picard et al., 2011; Vona et al., 2011; Picard et al., 2013). Using a variety of crystal shapes and sizes, all of the aforementioned papers showed that the abundance of crystals significantly increased the viscosity of the suspension and that aspect ratio and particle size must be taken into account. As an example, Picard et al. (2011, 2013) examined the effect that a high feldspar (tabular) content had on a two-phase magma. They found that feldspar crystal interactions dominated at a much lower crystal volume fraction (~ 0.3) compared to a magma with a high pyroxene or olivine (cubic) content (~ 0.5).

Analogue experiments on two-phase, crystal-melt mixtures enable variables to be systematically altered including liquid viscosity, crystal shape, density, size, and volume fraction. A number of papers investigated the effect of crystals on the apparent viscosity of the suspension

(e.g., Jeffery, 1922; Jeffrey and Acrivos, 1976; Mueller et al., 2010a, 2011). In particular, the experiments of Mueller et al. (2010a, 2011) examined a range of crystal sizes, aspect ratios and volume fraction to derive an empirical model for the apparent viscosity of a crystal-melt suspension. Based on the average aspect ratio and size, the formulation of Mader et al. (2013) (using the data from Mueller et al. (2010a, 2011)) can be used to determine the maximum packing fraction; an important parameter for developing yield strength (e.g., Hoover et al., 2001; Saar et al., 2001).

The relative effect of bubbles on a melt has been well characterised by experiments on analogue and natural samples (Bagdassarov and Dingwell, 1992, 1993; Bagdassarov et al., 1994; Manga et al., 1998; Lejeune et al., 1999; Manga and Loewenberg, 2001; Llewellin et al., 2002a,b; Rust and Manga, 2002; Pal, 2003; Llewellin and Manga, 2005). These authors showed that bubble shape is strongly controlled by strain rate, which in turn affects the viscosity. The capillary number (the ratio of viscous to restoring forces) therefore, is an important parameter when calculating the viscosity of a bubble-melt mixture. Bubbles that are spherical increase the viscosity while elongated bubbles reduce the viscosity (e.g., Llewellin et al., 2002b; Rust and Manga, 2002). In addition, samples that are subjected to shear at high temperature develop areas of strain localisation sub-parallel to the shear plane. These zones have been shown to focus permeability resulting in significant outgassing (e.g., Caricchi et al., 2011; Pistone et al., 2012).

Rheology experiments on natural samples have largely focussed on basalts (e.g., Ishibashi and Sato, 2007; Villeneuve et al., 2008; Ishibashi, 2009; Vona et al., 2011) or rhyolites (e.g., Bagdassarov and Dingwell, 1992, 1993; Bagdassarov et al., 1994), two end member compositions. A small number of studies have examined the multi-phase rheology of trachyte at high pressure and temperature (e.g., Caricchi et al., 2008; Picard et al., 2011, 2013; Vona et al., 2013). Importantly, there are very few that have examined the rheology of andesites. The specific case of andesite dome lavas at very high crystallinities and at atmospheric pressure has been examined by Lavallee et al. (2007) and Cordonnier et al. (2009). Therefore, a rheological assessment of natural andesite magma using existing physical models would provide a useful contribution to our understanding of andesitic eruptions. However, due to the limited number of rheological experiments on andesite magmas (Mader et al., 2013), it is possible that generic rheological models may require further experimental validation.

The studies discussed so far focus primarily on developing two-phase rheological models, involving either crystal and melt or bubbles and melt (see Mader et al., 2013 and references therein). Few studies exist of the more complex - and realistic - situation of three-phase suspen-

sions (e.g., Shields et al., 2014). These include the rheological study of synthetic high-viscosity magmas containing both crystals and bubbles (e.g., Pistone et al., 2012, 2013). More recently, Truby et al. (2014) present a constitutive model which uses the bubble suspension as an 'effective medium' in which the crystals reside, i.e. the apparent viscosity of the bubble suspension is used as the melt viscosity in the two-phase crystal suspension model. Rheological measurements of analogue three-phase suspensions of spheres and bubbles at low capillarity are shown to fit the model well. In this paper, we use a similar approach to that of Truby et al. (2014). Beckett et al. (2014) present a similar calculation for Stromboli basalts and show that there is no significant difference in the calculated viscosity whether the three-phase model is generated using the bubble suspension or the crystal suspension as the effective medium.

Small volume magmatic eruptions potentially provide insights into the minimum conditions required for magma to erupt. This is particularly important at volcanoes that commonly erupt small magma volumes interspersed between larger events. This is the case for Ruapehu, which makes it an excellent case study for this type of process. Historically, the typical erupted volumes are < 0.001 km^3. In addition, the mineralogy of Ruapehu magmas is relatively simple for an arc andesite, consisting of abundant plagioclase $\gg$ clinopyroxene and orthopyroxene $\pm$ Fe-Ti oxides (magnetite $\gg$ ilmenite) (Gamble et al., 1999; Price et al., 2012; Kilgour et al., 2013). Therefore, and combined with the bubble volume fraction, the rheology of the magma is approximated by a simple crystal population. The H_2O content of Ruapehu magmas is also very low (2 wt % H_2O; 1000 ppm CO_2), which also makes Ruapehu an interesting case to examine the physical properties of a relatively dry, arc andesite (Kilgour et al., 2013).

There has been no work published on the textures of historically-erupted scoria from Ruapehu. Therefore, the evolving physical state of the magma is not well constrained. For our study, we make some preliminary observations on the erupted scoria, which allows some estimates for the state of Ruapehu magma from storage to eruption. We use these to quantify the possible rheological properties at various stages, including storage processes of cooling and equilibrium crystallisation, and decompression during ascent. During decompression, we attempt to determine the magma rheology at a series of pressure steps, broadly similar to step-decompression experiments (e.g., Gardner et al., 1999; Couch et al., 2003a; Brugger and Hammer, 2010) and similar to the modelling approach of Baker and Alletti (2012), who examined the evolution of the volatile component of a notional magma during ascent. Modelling magma rheology as a continuous pressure drop is beyond the scope of this work, but in future, a more comprehensive account of bubble growth and crystallisation kinetics will make this possible. this will provide a

more comprehensive account of bubble growth and crystallisation kinetics. This work provides a simple, first-order, yet reasonable approximation of decompression, involving microlite crystallisation and bubble growth. We illustrate this method by calculating the evolving rheology of Ruapehu magma and attempt to account for the style and size duration of historical eruptions.

2. Framework for modelling magma evolution

To calculate the evolving rheology of Ruapehu magmas, we use a rather simple framework (Fig. 1). To this end, we consider a typical Ruapehu magma and examine the effect of decompression on crystallisation and gas exsolution. This includes an account of the changing composition of the melt phase due to crystallisation and bubble growth. By doing so, we then calculate the rheology of the melt as a Newtonian fluid (μ), and the apparent viscosities of the bubble-melt (η_b) and crystal-melt suspensions (η_{cr}). Using recently published constitutive equations, we then calculate the magma rheology (η).

We use a starting composition that is representative of erupted scoria from historical eruptions (Gamble et al., 1999; Kilgour et al., 2013) (Table. 1). We examine three representative Ruapehu magmas with different eruption temperatures (915, 977 and 1030 °C), which are determined by mineral-melt equilibria calculations (Kilgour et al., 2013). The melt composition is then calculated at a series of pressures under isothermal conditions, using the thermodynamic software - MELTS (Ghiorso and Sack, 1995; Asimow and Ghiorso, 1998). Calculations are conducted at variable pressure steps of between 10 and 100 MPa, depending on the relative changes in the model output. We then continue to decompress the magma until the composition of the liquid phase correlates well with the groundmass composition of the natural samples.

Our modelling approach assumes that the magma reaches its final melt composition at the point at which crystallisation ceased i.e. the magma erupted explosively. If further crystallisation occurs to a lower pressures, the crystal content is significantly higher than the scoria exhibits (the melt fraction would also be very low) and the groundmass glass composition becomes overly evolved. For example, continued decompression to low pressure replicates the crystallinity and liquid composition of dome lavas (c.f. Blundy et al., 2008).

2.1. Melt composition

During crystallisation, the residual melt composition evolves significantly. To investigate the changing melt composition due to crystallisation, and the resultant rheological effect, either experimental data or thermodynamic models are required. There are no published data on the

phase relations for Ruapehu magmas as a function of intensive variables, such as pressure and temperature. Although we performed a few limited experiments to confirm the melt vs. crystal proportions, these were very limited and not designed to determine the variation in melt composition for a large number of variable parameters. Until such a database exists, we are limited to using the program MELTS (Ghiorso and Sack, 1995; Asimow and Ghiorso, 1998) to determine the phase relations, melt fraction, and compositions based on equilibrium crystallisation (Ghiorso and Sack, 1995; Asimow and Ghiorso, 1998). We also assume that the magma is confined to a closed system, whereby there is no loss or gain of elements, heat, volatiles or crystals. MELTS is a thermodynamic model that calculates the phase assemblage, liquid composition and crystallinity given the bulk composition, temperature and pressure. The model has been calibrated against high pressure and temperature experiments on predominantly dry basaltic and rhyolitic compositions. The model tends to give a poor match to experimental data at high water contents where H_2O thermodynamic models are less well constrained. However, Ruapehu magmas are H_2O-poor and do not contain hornblende or biotite, which reduces the uncertainty of the MELTS calculations.

We test MELTS against our own experimental data from a powdered Ruapehu scoria sample along with andesites of a similar composition to Ruapehu (e.g., Blatter and Carmichael, 1998; Moore and Carmichael, 1998). This enables us to evaluate the ability of MELTS to determine phase relations and compositions for relatively dry, andesite magma. The model replicates the general phase relations and melt composition of the experimental data reasonably well. For example, Blatter and Carmichael (1998) ran a series of experiments at $\sim$ 100 MPa and 950-1100 °C; plagioclase and clinopyroxene proportions are in good agreement with those calculated by MELTS, while the calculated orthopyroxene proportions are lower. However, the melt fraction determined from the model is similar to that measured in experiments of Blatter and Carmichael (1998) and our own (Fig. 2). Calculated and experimental melt compositions are in good agreement for SiO_2, TiO_2, K_2O, and Al_2O_3. The model underestimates $FeO_{(T)}$, MgO, and CaO by $\sim$ 1 wt %, while it overestimates Na_2O by $\sim$ 1-2 wt % and H_2O by $<$ 1 wt %. When we propagate those values through to the Newtonian melt viscosity (μ) calculations of Giordano et al. (2008), we record an overestimation of ~ 0.3 log μ, which we consider as the errors involved in our calculations.

Using MELTS, we determine that for our starting composition and with the stated volatile content, the liquidus temperature is 1150 °C, given an initial pressure of 300 MPa (Ghiorso and Sack, 1995; Asimow and Ghiorso, 1998). This is taken from the maximum trapping pressures

calculated from phenocryst-hosted melt inclusions (Kilgour et al., 2013). We then cool three example magmas to their eruption temperature (915, 977, 1030 °C) and allow them to crystallise under equilibrium conditions. Once the eruption temperatures are reached, the magmas are decompressed (assuming adiabatic ascent) at variable stages. At each stage, the melt composition and crystal volume fraction are determined and input into the melt viscosity and rheological calculations.

2.2. Bubble content

While clast vesicularity data for Ruapehu scoria has been completed (see section 5.2), a thorough account of the bubble size distribution of Ruapehu scoria has yet to be attempted and is beyond the scope of this work. Nevertheless, we can approximate the bubble content, if we assume that all of the vapour that partitions from the melt is trapped in bubbles and is not lost through the development of bubble connectivity, leading to significant outgassing (e.g., Jaupart, 1998; Gonnermann and Manga, 2003). A similar approach was taken by Baker and Alletti (2012), who modelled the vesicularity and bulk volume of a modelled magma with decreasing pressure.

We use the volatile content of phenocryst-hosted melt inclusions from Kilgour et al. (2013) to represent the initial H_2O (2 wt %) and CO_2 (1000 ppm) content of the three model magmas. Based on the assumption of a closed system, we use the same bulk composition throughout. Using the solubility model of Papale et al. (2006), we then calculate the amount of vapour (wt %) in the system at a given pressure and temperature, using the melt composition output from the MELTS model. That solubility model is compositionally dependant, which is significant given the intermediate composition of Ruapehu magmas. The ideal gas law enables us to convert the wt % vapour in the system into a bubble volume and bulk density of the gas (Eqs 1 and 2). To determine the density of the melt, we use the formulation of Lange and Carmichael (1987) and Kress and Carmichael (1991). This takes into account the effect of pressure and thermal expansion. The results give a bubble volume (cm^3) per 100 g and as a result, we then obtain a bubble volume fraction. Clearly, this approach assumes ideal gas behaviour, which at high pressures is unlikely.

$$V = \frac{nRT}{P} \tag{1}$$

where V is the gas volume (m^3), n is the number of moles, R is the gas constant (J/mol/K), T is temperature (K) and P is pressure (Pa). Substituting density (ρ) into Eq. (1), (and where M

is the molar mass (g)) we are able to determine the density Eq. (2) and consequently, gas volume as a function of pressure and temperature (in our model, we consider only pressure changes).

$$\rho = \frac{PM}{RT} \tag{2}$$

To check if our ideal gas results are valid, we compare our results to the equation of state for binary (H_2O and CO_2) mixtures (Duan et al., 1992; Duan and Zhang, 2006), which accounts for non-ideality of mixing at high pressure and temperature. Their model is a complex physical chemical model and is based on a large number of high pressure and temperature experimental data. They computed a vast number of computer simulations to derive a universal equation of state that covers a broad temperature and pressure range. The Duan and Zhang (2006) model provides a useful tool to determine gas density and volume in addition to other parameters. When we compare the gas volumes derived from the ideal gas calculations with those from the equation of state (Duan and Zhang, 2006), they are in good agreement (i.e., within 15 % relative error to 40 MPa). At $>$ 40 MPa, the relative error increases from $\sim$ 15 to 60 % due to the non-ideality of mixing. However, the gas volume at pressure between 300 and 40 MPa is minimal ($<$ 1 cm^3) and consequently, the departure from ideality is considered insignificant for our purposes. Based on this comparison, we are confident that treating H_2O and CO_2 gases as an ideal mixture is valid at pressures $<$ 300 MPa and for this composition and volatile content.

The major advantage of this approach is that we can determine the bubble volume at any given pressure. This is in contrast to using the bubble size distribution (BSD) of an erupted scoria. A scoria BSD contains valuable information on late-stage bubble growth during vesiculation, however, the effect of coalescence needs to be considered in order to extract useful information on the evolution of bubbles in the magma. Without a detailed analysis of Ruapehu BSD's, we are restricted to model calculations. Nevertheless, unpublished vesicularity data from the 1995-1996 eruption episode is used to compare against the model output. None of the other eruptions analysed have sufficient samples in the archives to conduct a similar analysis.

Our modelling approach considers three magmas with identical bulk composition that are decompressed over the same pressure range. The only variable that has been altered between runs is magmatic temperature (i.e., 915, 977, and 1030 °C). Therefore, from Eqs. (1) and (2), magmatic temperature will have a minimal effect on the bubble volume fraction between magmas. Consequently, we use a single, representative bubble volume fraction vs pressure curve to calculate the changing bubble content during decompression.

2.3. Magma crystallinity

The crystal contents of the natural Ruapehu scoria are determined using two methods. Point counting is used to determine the phenocryst content, and for the microlites, we use both backscattered electron (BSE) images and major element compositional maps (following the method of Muir et al. (2012)) on a Hitachi S-3500N Scanning Electron Microscope (SEM) at the University of Bristol (Fig. 3). This enables us to quantify the size and abundance of each mineral phase and in some respects allows us to determine the impact of foreign crystal entrainment into the magma during ascent (i.e., using crystal size distribution analysis e.g., (Higgins, 2000, 2002; Muir et al., 2012). In order to convert the crystal content into a volume fraction, which is necessary for the rheological calculations, we use the following aspect ratios of 1:2:5 and 1:1:2 (short, intermediate, and long axes) for plagioclase and pyroxene phenocrysts respectively, and 1:1:7 for acicular pyroxene and plagioclase microlites. These values are similar to those determined for pahoehoe and a'a lava flows from Hawaii and Lava Butte (Hoover et al., 2001) that were then averaged for the numerical model of Saar et al. (2001). We then follow the method of Higgins (2000, 2002); Higgins and Chandrasekharam (2007), using the computer program *CSD-Corrections* (version 1.4.0.2) to convert two-dimensional greyscale images and element maps into three-dimensional crystal volume fractions. This enables us to calculate the relative viscosity effect of phenocrysts and microlites immediately before eruption. To account for crystal growth during ascent, we require a model that accounts for phase equilibria.

An erupted scoria contains varying amounts of microlites depending on the rate of decompression and undercooling (e.g., Couch et al., 2003a,b; Hammer, 2008). However, we have only limited information on the ascent rate prior to eruptions at Ruapehu and so we have chosen to exclude the effect of decompression or undercooling rates. To account for the growth of microlites, we use the output of MELTS to determine the crystallisation path. Ruapehu magmas are H_2O undersaturated, which means that crystallisation will be suppressed until the magma ascent path crosses H_2O saturation.

We assume a linear rate of crystal growth from H_2O saturation to the final crystal content, which we acknowledge to be a simplification of the kinetics of crystal growth (Fig. 4). However, using this method, we are able to determine the volume fraction of microlites, while phenocrysts were assumed to be stable throughout magma ascent (i.e., we ignored crystal resorption).

While we ignore decompression rate and the amount of undercooling, it is worth noting that these are important factors in driving microlite content and texture (see Hammer (2008) and Blundy and Cashman (2008) for a review of microlite growth kinetics). Furthermore, the analysis

of crystal size distributions is used to estimate growth rates, residence times and the extent of crystal inheritance (e.g., Marsh, 1988; Higgins, 2000, 2002). Hence, a more rigorous account of crystal growth in Ruapehu magmas requires a thorough CSD analysis and potentially, a number of high temperature and pressure experiments to constrain the phase equilibria. In future, this would be a useful contribution, but for this work, we attempt to simplify the system to provide a best-estimate of the absolute conditions.

3. Textural analysis of natural samples

To provide some background to the rheological modelling, we describe the key textures present in Ruapehu scoria as summarised in Tables 2, and 3 and Fig. 5. Ruapehu scoria from historical eruptions exhibit similar mineralogy (as mentioned above), mineral sizes and aspect ratios.

Phenocrysts sizes and aspect ratios are consistent between scoria samples. Plagioclase phenocrysts are up to 4 mm across, but more commonly $\sim$ 1-2 mm across. Their aspect ratio is $\sim$ 5:1 (length:width), while clinopyroxene and orthopyroxene phenocrysts are of a similar size (i.e., 1-2 mm across) and have a similar aspect ratio of $\sim$ 2:1.

The most notable difference between the scoria samples is the abundance of microlites. In particular, the 1969 eruption (915 °C) is microlite-free, while the 1977 (977 °C) and 1995 (1030 °C) eruptions contain 30 and 20 % microlites, respectively.

4. Methods

4.1. Experimental methods

Four phase equilibria experiments were conducted to determine the melt fraction of a representative Ruapehu magma at temperatures of 850, 900, 950, and 1000 °C. This enables us to compare the phase relations of Ruapehu against the thermodynamic predictions of the MELTS model (Ghiorso and Sack, 1995; Asimow and Ghiorso, 1998) and the experiments of Blatter and Carmichael (1998). The experiments of Blatter and Carmichael (1998) were conducted on a similar andesitic composition, but at higher temperatures (<1125 °C) compared to Ruapehu magmas of interest (915 - 1030 °C).

We used the whole rock powder of a Ruapehu scoria sample from the 1995-1996 eruptions of Ruapehu, which has a similar composition to other historical scoria samples (e.g., Gamble et al., 1999; Kilgour et al., 2013) (Table. 1). Each Au capsule had enough water added for the experiment to be H_2O-saturated and these were welded shut, then pressurised and heated

in either a Titanium-Zirconium-Molybdenum (TZM) pressure vessel (900, 950, and 1000 °C experiments) or a cold-seal apparatus (850 °C) at the University of Bristol, UK, both with rapid quench capabilities ($\sim$ 200 °C/s). For the TZM experiments, the pressure medium was a mixture of H-Ar gas, which allows for the oxygen fugacity to be buffered at $\sim$ nickel-nickel oxide (NNO). Each TZM experiment ran for 48 hours. The experiments in the cold-seal apparatus, at 850 °C, were pressurised with water and were run for 72 hours before being quenched. Although not controlled, the 'intrinsic' oxygen fugacity in these pressure vessels is netween NNO and NNO+1. Only those capsules that weighed the same before and after the experiment were considered successful. The melt fraction of each capsule was determined via image thresh-holding in *ImageJ* to estimate the proportions of crystals and glass.

4.2. Method for calculating three-phase rheology

To determine the evolving rheology of Ruapehu magmas, we use the two-phase models of Mader et al. (2013) at a series of discrete pressure steps. These models require a simple account of the bubble fraction (ϕ_b) or vesicularity, relative to the melt phase Eq. (3), and the crystal volume fraction (ϕ_{cr}) relative to the total volume Eq. (4). This allows us to directly calculate the three-phase rheology as a whole. To put it simply, our modelling takes a binary approach whereby we first calculate the bubble-melt suspension rheology (η_b) by ignoring crystals. We then take that rheology to represent the liquid phase, or effective medium, and add phenocrysts and finally microlites to obtain the three-phase magma rheology. Because this method is calculated using models for only two-phase suspensions, this approach neglects the potential non-ideal interactions that may occur between bubbles and crystals in a natural magma. Nevertheless, until a full three-phase model is developed, this is considered the most reasonable approach.

$$\phi_b = V_b/(V_b + V_m) \tag{3}$$

where V_b is the bubble volume and V_m is the total magma volume

$$\phi_{cr} = V_{cr}/(V_{cr} + V_m) \tag{4}$$

where V_cr is the crystal volume

4.2.1. Melt viscosity

The viscosity of a melt is strongly controlled by its composition. We use the model of Giordano et al. (2008) to calculate the Newtonian viscosity of the melt phase (μ). That model is empirical

and incorporates a large number of experimental data from a wide range of magma compositions, at atmospheric pressures. The model is strongly dependant on the major element composition and the H_2O and F content (in this case, these data were obtained by SIMS analysis - Kilgour et al. (2013)). The final melt viscosity of a magma is calculated from the groundmass glass composition of erupted scoria (Kilgour et al., 2013; Table 3). The initial liquid and its viscosity is determined from the bulk rock composition (Gamble et al., 1999; Kilgour et al., 2013) (Table. 1) above the liquidus temperature.

4.2.2. Rheology of a melt-bubble suspension

The rheology of a bubble-melt suspension is strongly dependant on the shape and size of the bubbles. It has been shown that spherical bubbles increase the viscosity of the suspension, while elongated bubbles create free-slip surfaces and therefore viscosity is reduced (Llewellin et al., 2002a,b; Rust and Manga, 2002; Mader et al., 2013). Bubble shape is governed by the ratio between the deforming, viscous stress and the restoring stress due to surface tension, termed the Capillary number (Ca). Therefore, a small Ca will result in spherical bubbles while for a large Ca, elongated bubbles are produced.

To simplify our rheological calculations including bubbles, we initially assume that there is either no flow (i.e., the bubbles are spherical) or rapid flow (i.e., the bubbles are elongated), which means that for this work, we only consider the bubble volume fraction and its effect on the bubble-melt rheology (assuming a closed system). This allows us to account for the end member effects of bubble shape on the apparent viscosity of the bubble suspension (η_r_b), which in the case of bubbles is categorised by Eqs. (7) and (8) (Mader et al., 2013).

$$\eta_{r\_b,o} = \mu(1-\phi)^{-1} \tag{5}$$

$$\eta_{r\_b,\infty} = \mu(1-\phi)^{\frac{5}{3}} \tag{6}$$

where ϕ_b is the bubble volume fraction given in Eq (3) and μ is the Newtonian viscosity of the melt phase.

It is usual to give the apparent viscosity as a dimensionless relative viscosity such that:

$$\eta_{r\_b,o} = (1-\phi)^{-1} \tag{7}$$

$$\eta_{r\_b,\infty} = (1-\phi)^{\frac{5}{3}} \tag{8}$$

These expressions provide the upper ($\eta_{r\_b,o}$) and lower ($\eta_{r\_b,\infty}$) limits of relative viscosity. $\eta_{r\_b,o}$ assumes that all bubbles are spherical and therefore increases the viscosity of a suspension in a similar fashion to a solid crystal, while $\eta_{r\_b,\infty}$ accounts for the effect of elongation, in equilibrium with the strain. As a result, the relative viscosity decreases.

While it is useful to model the system without considering a range in bubble sizes and the strain rate, it is clearly an artificial construct. The only constraints we have from ascent rate and therefore strain rate, are from diffusion chronometry (Kilgour et al., 2014). They showed that magma interactions that finally triggered each historical eruption at Ruapehu occurred within one month. These data provide an estimation of the ascent rate from the storage region, which is located between 2 and 9 km depth (Kilgour et al., 2013). Ideally, diffusion timescales are used in conjunction with pre-eruption seismicity, however, Bryan and Sherburn (1999) showed that prior to the 1995 and 1996 eruptions of Ruapehu, seismicity was minor and inconsistent. Therefore, we are restricted to using the end member effects of bubbles at high ($\eta_{r\_b,\infty}$) and low ($\eta_{r\_b,o}$) capillary number.

4.2.3. Rheology of a melt-crystal suspension

The effect that crystals exert on the suspension viscosity has been largely determined from analogue experiments involving a variably viscous liquid phase, and glass or ceramic beads of varying sizes and shapes (Mueller et al., 2010b). Other experiments were conducted on synthetic magmas at high temperature and pressure (Caricchi et al., 2007), which were then built into a model that considered the influence of crystals on a suspension viscosity (Costa et al., 2009). For consistency, we have accounted for the effect of crystals (and bubbles) on the relative viscosity (η_{r_cr}) using the equations of Mader et al. (2013), which are mainly based on Mueller et al. (2010a, 2011). A series of steps are required to determine the relative effect of crystals, which take into account the shape, size and maximum packing fraction of crystals within the suspension.

Firstly, it is necessary to determine the maximum packing fraction (ϕ_m) using Eq (9). We assume that crystals are rough particles (i.e., ϕ_{m_1} and b are 0.55 and 1 respectively), which is reasonable for natural crystal shapes (Mader et al., 2013).

This leads to

$$\phi_m = \phi_{m_1} exp\left[-\frac{(log_{10} r_p)^2}{2b^2}\right] \tag{9}$$

where r_p is the crystal aspect ratio.

Using a modified Maron-Pierce equation, the relative consistency (K_r) (analogous to relative apparent viscosity i.e., K/μ) will depend on the crystal content (ϕ_{cr}) with respect to ϕ_m, thus

$$K_r = \left(1 - \frac{\phi_{cr}}{\phi_m}\right)^{-2} \tag{10}$$

According to Mader et al. (2013), if $\phi_{cr}/\phi_m < 0.5$, then $\eta_{r\_cr} = K_r$, because the rheology is adequately considered to be behaving as a Newtonian fluid. If $0.5 < \phi_{cr}/\phi_m < 0.8$, then η_{cr} requires a power law to describe the magma rheology (Eq 11) due to the effect of shear thinning. This is clearly only valid for very dilute suspensions. At high crystal contents, the rheology of the suspension must account for non-Newtonian behaviour. Consequently, the Herschel-Bulkley equation considers the strain rate and the development of a yield stress (Eq 12).

$$\eta_{r\_cr} = K_r \dot{\gamma}^{n-1} \tag{11}$$

where $\dot{\gamma}$ is strain rate and n is the flow index, which considers the aspect ratio and crystal content of the magma.

At high crystal content i.e., when $\phi_{cr}/\phi_m > 0.8$, yield stress (τ) must be overcome and as a result, the Herschel-Bulkley equation is used to determine the magma rheology.

$$\tau = \tau_o + K\dot{\gamma}^n \tag{12}$$

where τ_o is yield stress at which flow may commence and K is consistency.

To account for the effect of shear thinning due to crystal alignment, Mueller et al. (2010a) developed an empirical model (Eq. 13) for the flow index (n) as

$$n = 1 - 0.2 r_p \left(\frac{\phi_{cr}}{\phi_m}\right)^4 \tag{13}$$

5. Results

5.1. Melt composition and viscosity

Using MELTS to determine the melt composition during decompression, we model the changing melt viscosity through time (Fig. 6a and d). As expected, crystallisation causes the melt to chemically evolve (Fig. 6b). From 300 to 100 MPa, minor resorption results in a very small change in the melt composition. This results in a slight increase in melt fraction as pressure is

reduced (Fig. 6c). With continued decompression (< 100 MPa), extensive crystallisation leads to increased SiO_2 and H_2O, two elements that exert a strong control on melt viscosity (Giordano et al., 2008). In this work, we ignore the effects of small variations in F during decompression as the variations in F abundance are small (Kilgour et al., 2014). The three model magmas crystallise inversely proportional to their magmatic temperatures. For example, the SiO_2 content (a simple proxy for melt evolution) at temperatures of 1030, 977 and 915 °C increases upon decompression by 2, 4 and 5 wt % respectively (Figs. 6a and b). We also note that the onset of rapid crystallisation (i.e., the rapid change in slope within the SiO_2 vs Pressure plot) occurs at much lower pressures in the 1030 °C magma ($\sim$ 50 MPa) compared to the lower temperature magmas (i.e., $\sim$ 80 MPa - 977 °C and $\sim$ 100 MPa - 915 °C) (Fig. 6). This variation in crystallisation with pressure is reflected in the change in melt fraction. For the 1030 °C magma, the melt fraction decreases from 0.82 to 0.71 from 40 to 25 MPa (within 15 MPa), while a similar decrease in melt fraction occurs over a 25 and 50 MPa pressure range for the 977 (0.62 to 0.52) and 915 (0.52 to 0.41) °C melts respectively.

As a consequence of crystallisation and the resultant change in melt composition, the melt viscosity changes significantly. Because each magma is modelled at different temperatures, the initial viscosity of each magma is different. The initial melt viscosity for the 915 °C magma is $\log \mu = 4.4$, where μ is in Pa s. For the 977 °C and 1030 °C magmas, the initial melt viscosity is $\log \mu = 3.9$ and $\log \mu = 3.3$, respectively. Broadly similar to the SiO_2 trend, $\log \mu$ of the residual melts for all temperatures increases rapidly at the onset of significant crystallisation, due to the evolution of the melt phase ($\sim$ 100 to 50 MPa). The viscosity increase due to crystallisation is variable, depending on magmatic temperature. An increase of $\sim$ 1.7 (915 °C), $\sim$ 1.2 (977 °C), and $\sim$ 0.7 Pa s (1030 °C) log units is observed (Fig. 6) for each of the modelled magmas.

5.2. Effect of bubbles on viscosity

The volatile content (2 wt % H_2O and 1000 ppm CO_2) of all three modelled Ruapehu magmas is kept constant; the only parameter that varies between the runs is the magmatic temperature. The variation in bubble volume fraction with pressure is also the same in all models (Fig. 7). From 300 to $\sim$ 50 MPa, the bubble volume fraction is minimal. At $\sim$ 50 MPa, a rapid increase in bubble volume fraction, due to bubble expansion and exsolution of volatiles from the magma occurs to $\sim$ 0.55 at 5 bars (near atmospheric pressure). We investigate the rheological effect of an increased volatile content for the same bulk composition (3, 4, and 5 wt % H_2O with no increase in CO_2). There appears to be minimal difference between the 2 and 3 wt % H_2O runs, but with

more volatiles (4 and 5 wt%), the differences are more marked. For the 5 wt % H_2O run, bubbles begin to form at $\sim$ 150 MPa, while for the 4 wt % H_2O run, bubble formation begins at $\sim$ 100 MPa. All volatile-rich ($>$ 3 wt % H_2O) runs reach a final bubble volume fraction of 0.7 to 0.8 at 5 MPa.

We compare the modelled bubble volume fractions against existing unpublished data from the 1995-1996 eruption scoria. This dataset involved the measurement of the bubble volume fraction of more than 200 individual scoria clasts (courtesy of M. Rosenberg *pers. comm.*) using the Archimedes method (Houghton and Wilson, 1989). Figure 8 shows that the bulk of the subunits record a range between 0.3 and 0.7, with an overall mean of $\sim$ 0.55. This is in excellent agreement with the modelled data for the 2 wt % H_2O magma.

As a consequence of gas expansion, the bulk volume of the magma increases substantially at low pressures (Fig. 9). Gas expansion occurs at higher pressures in the volatile-rich simulations and as a result, the bulk magma volume increases at higher pressures than the volatile-poor runs. As with the bubble volume fraction data, the final magma volume is similar between all modelled magmas.

Changes in relative viscosity (η_b) due to bubbles, alongside the bubble volume fraction (ϕ_b) are shown in Figure 10. The range in η_b increases with decreasing pressure because of the disparate effect of bubble shape (due to capillary number) as the bubble fraction becomes large. At very low pressures, where $\phi_b \rightarrow 0.6$, the divergence in η_r_b ranges from $\sim$ 0.2 to 2.6. The point at which fragmentation likely occurs ($\sim$ 25 MPa) has a range in η_r_b of $\sim$ 0.75. At greater confining pressures, $\eta_b \rightarrow 1$ for both the upper ($\eta_{r\_b,\infty}$) and lower ($\eta_{r\_b,o}$) endmembers, which is to be expected as bubbles are not added to the magma until H_2O saturation.

5.3. Effect of crystals on viscosity

Ruapehu groundmass glass is variably populated by microlites (crystals $<$ 100 μm) consisting of plagioclase, clinopyroxene and orthopyroxene. Within the microlite population, plagioclase and pyroxene form acicular laths (typically on the order $\sim$ 5 to 20 μm long) with average aspect ratios (r_p) $\sim$ 7. From greyscale BSE images of the most microlite-bearing glass (Fig. 3), we obtain an average area fraction for pyroxene $\sim$ 0.16 and for plagioclase $\sim$ 0.10. Using *CSDCorrections*, we determined a microlite volume fraction (ϕ_{cr}) of $\sim$ 0.3. Using the same method for the 977 °C magma, ϕ_{cr} = 0.2 and for the 915 °C magma, the glass is considered microlite-free (i.e., ϕ_{cr} = 0).

We assume a linear microlite growth rate from H_2O saturation to the final crystallinity (Fig.

4). This enables us to estimate the crystal volume fraction as a function of pressure. For the 915 °C magma, the rheology of the two-phase suspension is simplified to the viscosity of the melt and the relative viscosity due to the addition of phenocrysts. Figure 4 shows the evolution of microlite content with pressure, under isothermal conditions. The onset of crystallisation occurs at relatively low pressures ($\sim$ 50 MPa) for the 1030 °C magma compared to the 977 °C magma ($\sim$ 80 MPa). In addition, the growth rate of the 1030 °C magma is significantly faster than the 977 °C magma.

The effect of differing microlite growth rates causes significant changes to η_{cr}. We consider three different strain rates ($\dot{\gamma}$) of 0.1, 1, and 10 s^{-1}, and for the 1030 °C magma, η_{cr} ranges from $\sim$ 2 - 50, while for the 977 magma the range is $\sim$ 2 to 5. Using Eq.(11), the effect of large η_{cr} due to microlite growth causes the viscosity (log η) to increase by $\sim$ 1.5 to 2 log units (Fig.11).

The phenocryst (crystals $>$ 500 μm) assemblage of Ruapehu scoria is dominanted by plagioclase ($\sim$ 0.20 area fraction) with subordinate orthopyroxene ($\sim$ 0.05) and clinopyroxene ($\sim$ 0.05). Based on point counting, the area fraction of these phenocrysts is similar in all scoria analysed at $\sim$ 0.30 to 0.35. Combined with the aspect ratio of typical plagioclase (1:2:5) and pyroxene (1:1:2) crystals, we obtain a phenocryst volume fraction of $\sim$ 0.35. Because we consider phenocrysts to be a static phase, and using Eq (11), η_{cr} is constant with decreasing pressure at $\sim$ 3, 8, and 20 for $\dot{\gamma}$ of 0.1, 1, and 10 s^{-1} respectively.

The effect of phenocrysts and microlites on the magma viscosity are shown in Figure 11. The addition of phenocrysts to the melt phase results in a viscosity increase of $\sim$ 1 log unit in all three magmas. Shallow microlite crystallisation, with the addition of phenocrysts, leads to a viscosity increase of $\sim$ 2 log units above the melt viscosity. The final apparent viscosity (log η_{cr}) of all three magmas is between 6 and 7 (i.e., 10^6 - 10^7 Pa s).

6. Discussion

6.1. Implications of MELTS modelling for three-phase rheology

The MELTS model reproduces the mineral assemblage and melt composition of Ruapehu scoria reasonably well and this suggests that Ruapehu magmas can be modelled under equilibrium conditions to low pressures (<25 MPa). The best match between the model outputs and the natural scoria (groundmass glass composition and melt fraction) is achieved at $\sim$ 25 to 30 MPa ($\sim$ 1 km depth) for all three explosively erupted magmas. Therefore, Ruapehu magmas are inferred to have ascended until $\sim$ 25-30 MPa ($\sim$ 1 km below the crater floor). From this depth, we suggest

that rapid ascent occurred soon before each eruption. Hurst (1998) showed that the base of the active hydrothermal system extends to $\sim$ 1 km and this may suggest that eruptions are driven in part by the interaction of magma and the active hydrothermal system. These implied magma-water interactions increase the potential to generate phreatomagmatic and phreatic eruptions at Ruapehu (e.g., Kilgour et al., 2010). Alternatively, rapid ascent may occur at this level due to vesiculation (see below).

By combining the bubble-melt suspension rheology with crystals (both microlites and phenocrysts), we calculate an approximate three-phase rheology for Ruapehu magmas. η_r_b for the bubble-melt suspension varies with pressure from $\sim$ 0.2 to 2.6, while η_{r_cr} for the crystal-melt suspension ranges from $\sim$ 1 to 1000, which is strongly strain rate ($\dot{\gamma}$) dependent. By combining the two relative viscosities, the three-phase magmas (*eta*) span log $\eta \sim 4$ to 6.4, significantly higher than the melt viscosity (Fig. 12). Crystals exert a much greater influence on magma rheology than bubbles and hence, magma ascent dynamics are principally controlled by the amount and composition of the evolving crystal assemblage. A full understanding of crystal kinetics will inevitably improve the accuracy of the rheology as a function of depth. Nevertheless, our simple linear relationship seems to model the evolving crystal assemblage well and we can therefore draw conclusions with some confidence.

Extensive crystallisation occurs at relatively shallow depths for H_2O undersaturated andesite magmas. This is because a magma will only begin to crystallise when it becomes H_2O saturated (Blundy and Cashman, 2001). Ruapehu magmas are relatively dry compared to other arc andesites (Wallace, 2005; Kilgour et al., 2013) and as a consequence, crystallisation is suppressed during ascent. According to MELTS, Ruapehu magmas encounter H_2O saturation at low pressures ($\sim$ 100 and 40 MPa), before the onset of crystallisation.

6.2. Ruapehu magmas: erupt or stall?

Textural analysis of historical Ruapehu scoria shows that the phenocryst abundance ($\sim$ 30 %) and proportions are similar between eruptions, while the microlite content is variable (Table. 2). Importantly, because plagioclase is the dominant mineral phase (i.e., 15 vol %), the relatively high aspect ratio has a significant effect on the magma rheology. Therefore, with a phenocryst content of $\sim$ 30 %, and from Mueller et al. (2010a), yield stress develops when the crystal volume fraction is more than 80 % of the maximum packing fraction (i.e., $\phi_{cr}/\phi_m > 0.8$), our calculations show that there is no yield stress developed until microlite growth because ($\phi_{cr}/\phi_m = 0.70$, when $r_p = 5$). Because ϕ_m is strongly dependant on the aspect ratio (r_p), it is possible

that the mixed pyroxene and plagioclase crystal population results in a lowered average aspect ratio, and therefore a reduced ϕ_m. This then would allow for further microlite growth before a yield stress is developed.

Once microlites are added to the overall crystal content of the magma, yield stress will almost certainly develop. From the textural analysis, microlites are generally high aspect ratio crystals (i.e., $r_p \leq 5$), which with limited crystallisation, would decrease ϕ_m and result in a yield stress. Indeed, any microlite growth, for instance during decompression-driven crystallisation in the shallow subsurface (e.g., Blundy and Cashman, 2001) would clearly result in the development of a yield stress. As a result, the magma is very likely to stall unless driving pressures and strain rates ($\dot{\gamma}$) were high. At high $\dot{\gamma}$ (> 10 s^{-1}), shear thinning would result in a lower apparent viscosity (due to crystal alignment and crystal fracturing) and potentially enable continued flow to eruption. However, if $\dot{\gamma}$ were low (< 0.1 s^{-1}), the magma would be unable to flow without first overcoming the yield strength. This implies that the strain rates at Ruapehu must be relatively high in order for these magmas to erupt. However, the strain rates are unlikely to be very high as there is no clear microlite alignment, which would be likely under high strain conditions.

The large effect of crystals on magma rheology can partly explain the transition from effusive to explosive behaviour in a range of settings and for a wide range in magma compositions. Caricchi et al. (2008) examined the products of the Monte Nuovo eruption (trachyte) and found that strombolian episodes were driven by high overpressures within a relatively low crystal content ($\phi_{cr} \sim$ 0.2-0.3) magma, while the explosive event that followed, had $\phi_{cr} \sim$ 0.4-0.6. They suggested that extensive crystallisation prior to the violent explosion created a plug of highly viscous magma within the upper conduit. This formed a barrier to gas flow, eventually generating a pressurised gas pocket beneath the plug. This plug eventually failed, resulting in a Vulcanian eruption (Caricchi et al., 2008). At Mt Etna, Giordano et al. (2010) modelled basaltic ascent within the conduit and showed that the style of basaltic eruptions was strongly influenced by the crystal content (due to variable crystallisation rates) of magma. They concluded that the transition from fire-fountaining to strombolian eruption styles was determined by the presence of a crystal-rich cap to the magma column. If present, this crystal-rich magma cap would act to destabilise the system and favour strombolian eruptions. The absence of a magma plug would favour fire-fountaining due to the free expansion of volatiles at low pressures.

Because Ruapehu magmas are H_2O undersaturated, the suppression of microlite crystallisation (and the development of a yield stress) until the magma ascends to low pressures increases the potential for Ruapehu magmas to erupt. This is in contrast to H_2O saturated ('wet')

arc andesites. Undersaturated magmas ascend without decompression crystallisation occurring until gas expansion begins to drive rapid ascent and fragmentation. In contrast, H_2O saturated magmas crystallise continuously during ascent. As a consequence, H_2O saturated magmas must ascend fast enough that high undercoolings and rapid decompression inhibit crystal growth (Cashman and Blundy, 2000).

The presence of an active hydrothermal system and a large crater lake, coupled with the ability for H_2O undersaturated magmas to ascend, increases the potential for magma-water interactions at Ruapehu. If we assume a constant volume of relatively cool water, the interaction between Ruapehu magma and the hydrothermal system will generally result in a low magma:water ratio. This will inevitably lead to phreatomagmatic or phreatic eruption styles (e.g., Houghton et al., 1987; Hackett and Houghton, 1989; Johnston et al., 2000; Kilgour et al., 2010). This style of eruption is clearly dominant at Ruapehu (Scott, 2013; Kilgour et al., 2014), whereby only a small minority of eruptions are magmatic. These only occurred after Crater Lake had been expelled due to prolonged phreatomagmatic eruptions (e.g., 1995-1996 eruption episode).

From ~ 50 MPa, our calculations show that gas expansion (bubble growth) takes place rapidly. Without appreciable gas-loss, an increased bubble volume fraction within an increasingly viscous magma will generate significant bubble overpressures. As the bubble volume fraction continues to increase with decreasing pressure, gas expansion will cause the overall magma volume to increase, or if the overpressure exceeds the strength of the surrounding melt, the magma will fragment. This will almost certainly depend on the glass transition, coupled with the additional strength of crystals.

From our simple calculations, the expansion of bubbles will only begin when the magma has reached a pressure of < 50 MPa. At this pressure, an initial overpressure will start to drive magma ascent. Gas loss along conduit walls (e.g., Rust et al., 2004; Jaupart, 1998) or through a gas permeable network (e.g., Melnik et al., 2005) will significantly reduce gas overpressure and this may result in a more effusive eruption. From our results, extensive crystallisation due to nucleation-dominated crystal growth (e.g. Hammer and Rutherford, 2002), occurs at slightly higher pressures than significant (i.e., $\phi_b > 0.3$) bubble growth. Therefore, bubbles will begin to grow in an increasingly viscous melt-crystal suspension. A consequence of this will be hindered gas expansion, which will exacerbate the potential for bubble overpressure. This may explain why most Ruapehu eruptions are explosive, if not large volume.

6.3. Rheological impact of magma interactions

In a simple magmatic system, whereby the ascent of a buoyant magma occurs in effective isolation, we have shown that magma rheology can be calculated in a relatively straightforward manner using Mader et al. (2013). However, it is clear that ascending magma often interacts with other magmas or crystal mush zones (Nakamura, 1995; Nakagawa et al., 1999, 2002; Kilgour et al., 2013). Research into the dynamics of magma-magma and magma-mush interactions is ongoing, but a clear consequence of this process is the addition of foreign crystals along with more evolved melt into the rising magma. The additional input of crystals will greatly increase the apparent viscosity of the magma. These magmatic interactions will cause the apparent viscosity of the magma to increase dependant on the efficacy of the mixing process. In some cases, this may lead to the build-up of large tracts of high level, failed intrusions.

7. Conclusions

We have determined the rheology of Ruapehu magma from storage to eruption by characterising the bulk, crystal, and glass compositions, and volatile content of recently erupted Ruapehu scoria. We input these data into the thermodynamic model MELTS, to track the liquid composition and crystal content with decreasing pressure (300 to $\sim$ 25 MPa). From the melt composition, we were able to determine the melt viscosity using Giordano et al. (2008). We then examined the relative viscosity of crystals and bubbles in order to assess the evolution of magma rheology.

Using the model of Mader et al. (2013), we showed that crystals exert a much more significant control on the apparent magma viscosity compared to the addition of bubbles. As a result, the rheology of a magma will be largely determined by the amount and rate of crystallisation during ascent. High crystal growth rates may cause a magma to develop a yield strength, potentially resulting in a stalled plug of magma, while limited crystal growth will more readily promote weak strombolian eruptions.

Ruapehu magmas are H_2O undersaturated for most of their ascent history. Therefore, crystallisation is suppressed until the magma reaches saturation. According to the outputs from MELTS, this results in extensive crystallisation at 100 to 50 MPa, at significantly lower pressures than for a similar composition, yet H_2O saturated andesite. Due to this delay in crystallisation, Ruapehu magmas are more likely to erupt and this partly explains the high frequency and small volume of historical eruptions.

The microlite content of Ruapehu scoria is variable and because they significantly increase the apparent viscosity of the magma, an understanding of the kinetics of crystal growth in undersaturated Ruapehu magmas would greatly enhance our model and increase our understanding of the processes involved. Undersaturated crystallisation is suppressed until low pressures (100 to 50 MPa) and so it should be possible to use continuous decompression experiments to constrain microlite textures and abundance. This, in turn could be used as a geospeedometer that could determine magma ascent rates at Ruapehu. For instance, scoria from the 1969 eruption are microlite-free, while the 1996 scoria has a microlite volume fraction of ~ 0.3. From this, two key questions arise 1) are magmas ascending at different rates? and 2) what are those ascent rates? Determining these constraints would be a valuable study, which we hope will be conducted in the near future.

8. Acknowledgements

This work was funded by the New Zealand Ministry of Science and Innovation (MSI) Geological Hazards Programme (GHZ) in the form of a PhD studentship to GK at the University of Bristol. JB is supported by ERC Advanced Grant CRITMAG and a Royal Society Wolfson Research Merit Award. We would also like to thank Luca Caricchi for discussions on magma rheology and Chris Mathew for technical assistance. We thank Bruce Houghton for use of the clast vesicularity data held at GNS Science. The comments of an anonymous reviewer and A. Vona were very positive and thorough, which significantly improved the clarity of the final version.

9. References

Asimow, P. D. and Ghiorso, M. S. (1998). Algorithmic modifications extending MELTS to calculate subsolidus phase relations. *American Mineralogist*, 83:1127–1132.

Bagdassarov, N. and Dingwell, D. (1992). A rheological investigation of vesicular rhyolite. *Journal of Volcanology and Geothermal Research*, 50(3):307 – 322.

Bagdassarov, N., Dingwell, D., and Webb, S. (1994). Viscoelasticity of crystal- and bubble-bearing rhyolite melts. *Physics of the Earth and Planetary Interiors*, 83(2):83 – 99.

Bagdassarov, N. S. and Dingwell, D. B. (1993). Frequency dependent rheology of vesicular rhyolite. *Journal of Geophysical Research: Solid Earth*, 98(B4):6477–6487.

Baker, D. R. and Alletti, M. (2012). Fluid saturation and volatile partitioning between melts and hydrous fluids in crustal magmatic systems: The contribution of experimental measurements and solubility models. *Earth-Science Reviews*, 114(34):298 – 324.

Beckett, F., Burton, M., Mader, H., Phillips, J., Polacci, M., Rust, A., and Witham, F. (2014). Conduit convection driving persistent degassing at basaltic volcanoes. *Journal of Volcanology and Geothermal Research*, 283:19 – 35.

Blatter, D. L. and Carmichael, I. S. E. (1998). Plagioclase-free andesites from Zitácuaro (Michoacán), Mexico: petrology and experimental constraints. *Contributions to Mineralogy and Petrology*, 132(2):121–138.

Blundy, J. and Cashman, K. (2001). Ascent-driven crystallisation of dacite magmas at Mount St Helens, 1980-1986. *Contributions to Mineralogy and Petrology*, 140:631–650.

Blundy, J. and Cashman, K. (2008). Petrologic reconstruction of magmatic system variables and processes. *Reviews in Mineralogy and Geochemistry*, 69(1):179–239.

Blundy, J., Cashman, K., and Berlo, K. (2008). Evolving magma storage conditions beneath Mount St. Helens inferred from chemical variations in melt inclusions from the 1980-1986 and current (2004-2006) eruptions. *US Geological Survey professional paper*, (1750):755–790.

Bottinga, Y. and Weill, D. F. (1970). Densities of liquid silicate systems calculated from partial molar volumes of oxide components. *American Journal of Science*, 269(2):169–182.

Bottinga, Y. and Weill, D. F. (1972). The viscosity of magmatic silicate liquids; a model calculation. *American Journal of Science*, 272(5):438–475.

Brugger, C. R. and Hammer, J. E. (2010). Crystallization kinetics in continuous decompression experiments: Implications for interpreting natural magma ascent processes. *Journal of Petrology*, 51(9):1941–1965.

Bryan, C. and Sherburn, S. (1999). Seismicity associated with the 1995-1996 eruptions of Ruapehu volcano, New Zealand: narrative and insights into physical processes. *Journal of Volcanology and Geothermal Research*, 90(12):1 – 18.

Caricchi, L., Burlini, L., Ulmer, P., Gerya, T., Vassalli, M., and Papale, P. (2007). Non-Newtonian rheology of crystal-bearing magmas and implications for magma ascent dynamics. *Earth and Planetary Science Letters*, 264(34):402 – 419.

Caricchi, L., Giordano, D., Burlini, L., Ulmer, P., and Romano, C. (2008). Rheological properties of magma from the 1538 eruption of Monte Nuovo (Phlegrean Fields, Italy): An experimental study. *Chemical Geology*, 256(34):158 – 171.

Caricchi, L., Pommier, A., Pistone, M., Castro, J., Burgisser, A., and Perugini, D. (2011). Strain-induced magma degassing: insights from simple-shear experiments on bubble bearing melts. *Bulletin of volcanology*, 73(9):1245–1257.

Cashman, K. and Blundy, J. (2000). Degassing and crystallization of ascending andesite and dacite. *Philosophical Transactions of the Royal Society of London. Series A:Mathematical, Physical and Engineering Sciences*, 358(1770):1487–1513.

Cordonnier, B., Hess, K.-U., Lavallee, Y., and Dingwell, D. (2009). Rheological properties of dome lavas: Case study of Unzen volcano. *Earth and Planetary Science Letters*, 279(34):263 – 272.

Costa, A., Caricchi, L., and Bagdassarov, N. (2009). A model for the rheology of particle-bearing suspensions and partially molten rocks. *Geochem. Geophys. Geosyst.*, 10(3):Q03010–.

Couch, S., Harford, C. L., Sparks, R. S. J., and Carroll, M. R. (2003a). Experimental constraints on the conditions of formation of highly calcic plagioclase microlites at the Soufriére Hills Volcano, Montserrat. *Journal of Petrology*, 44(8):1455–1475.

Couch, S., Sparks, R. S. J., and Carroll, M. (2003b). The kinetics of degassing-induced crystallization at Soufriére Hills Volcano, Montserrat. *Journal of Petrology*, 44(8):1477–1502.

Duan, Z., Møller, N., and Weare, J. H. (1992). An equation of state for the CH_4-CO_2-H_2O system: II. Mixtures from 50 to 1000 °C and 0 to 1000 bar . *Geochimica et Cosmochimica Acta*, 56(7):2619 – 2631.

Duan, Z. and Zhang, Z. (2006). Equation of state of the H_2O, CO_2, and H_2O-CO_2 systems up to 10 GPa and 2573.15 K: Molecular dynamics simulations with ab initio potential surface. *Geochimica et Cosmochimica Acta*, 70(9):2311 – 2324.

Gamble, J., Wood, C., Price, R., Smith, I., Stewart, R., and Waight, T. (1999). A fifty year perspective of magmatic evolution on Ruapehu Volcano, New Zealand: verification of open system behaviour in an arc volcano. *Earth and Planetary Science Letters*, 170(3):301 – 314.

Gardner, J. E., Hilton, M., and Carroll, M. R. (1999). Experimental constraints on degassing of magma: isothermal bubble growth during continuous decompression from high pressure. *Earth and Planetary Science Letters*, 168(12):201 – 218.

Ghiorso, M. S. and Sack, R. O. (1995). Chemical mass transfer in magmatic processes IV. A revised and internally consistent thermodynamic model for the interpolation and extrapolation of liquid-solid equilibria in magmatic systems at elevated temperatures and pressures. *Contributions to Mineralogy and Petrology*, 119:197–212.

Giordano, D. and Dingwell, D. B. (2003). Non-arrhenian multicomponent melt viscosity: a model. *Earth and Planetary Science Letters*, 208(34):337 – 349.

Giordano, D., Polacci, M., Papale, P., and Caricchi, L. (2010). Rheological control on the dynamics of explosive activity in the 2000 summit eruption of Mt. Etna. *Solid Earth*, 1(1):61–69.

Giordano, D., Romano, C., Dingwell, D., Poe, B., and Behrens, H. (2004). The combined effects of water and fluorine on the viscosity of silicic magmas. *Geochimica et Cosmochimica Acta*, 68(24):5159 – 5168.

Giordano, D., Russell, J. K., and Dingwell, D. B. (2008). Viscosity of magmatic liquids: A model. *Earth and Planetary Science Letters*, 271(14):123 – 134.

Gonnermann, H. M. and Manga, M. (2003). Explosive volcanism may not be an inevitable consequence of magma fragmentation. *Nature*, 426(6965):432–435.

Gonnermann, H. M. and Manga, M. (2007). The fluid mechanics inside a volcano. *Annual Review of Fluid Mechanics*, 39(1):321–356.

Hackett, W. R. and Houghton, B. F. (1989). A facies model for a quaternary andesitic composite volcano: Ruapehu, New Zealand. *Bulletin of Volcanology*, 51:51–68.

Hammer, J. E. (2008). Experimental studies of the kinetics and energetics of magma crystallization. *Reviews in Mineralogy and Geochemistry*, 69(1):9–59.

Hammer, J. E. and Rutherford, M. J. (2002). An experimental study of the kinetics of decompression-induced crystallization in silicic melt. *Journal of Geophysical Research: Solid Earth*, 107(B1):ECV 8–1–ECV 8–24.

Higgins, M. D. (2000). Measurement of crystal size distributions. *American Mineralogist*, 85(9):1105–1116.

Higgins, M. D. (2002). Closure in crystal size distributions (CSD), verification of CSD calculations, and the significance of CSD fans. *American Mineralogist*, 87(1):171–175.

Higgins, M. D. and Chandrasekharam, D. (2007). Nature of sub-volcanic magma chambers, Deccan Province, India: Evidence from quantitative textural analysis of plagioclase megacrysts in the Giant Plagioclase Basalts. *Journal of Petrology*, 48(5):885–900.

Hoover, S., Cashman, K., and Manga, M. (2001). The yield strength of subliquidus basalts - experimental results. *Journal of Volcanology and Geothermal Research*, 107(13):1 – 18.

Houghton, B. and Wilson, C. (1989). A vesicularity index for pyroclastic deposits. *Bulletin of Volcanology*, 51(6):451–462.

Houghton, B. F., Latter, J. H., and Hackett, W. R. (1987). Volcanic hazard assessment for Ruapehu composite volcano, taupo volcanic zone, New Zealand. *Bulletin of Volcanology*, 49:737–751.

Hui, H. and Zhang, Y. (2007). Toward a general viscosity equation for natural anhydrous and hydrous silicate melts. *Geochimica et Cosmochimica Acta*, 71(2):403 – 416.

Huppert, H. and Sparks, R. (1981). The fluid dynamics of a basaltic magma chamber replenished by influx of hot, dense ultrabasic magma. *Contributions to Mineralogy and Petrology*, 75(3):279–289.

Hurst, A. W. (1998). Shallow seismicity beneath Ruapehu Crater Lake: results of a 1994 seismometer deployment. *Bulletin of Volcanology*, 60:1–9.

Ishibashi, H. (2009). Non-Newtonian behavior of plagioclase-bearing basaltic magma: Subliquidus viscosity measurement of the 1707 basalt of Fuji volcano, Japan. *Journal of Volcanology and Geothermal Research*, 181(12):78 – 88.

Ishibashi, H. and Sato, H. (2007). Viscosity measurements of subliquidus magmas: Alkali olivine basalt from the Higashi-Matsuura district, Southwest Japan. *Journal of Volcanology and Geothermal Research*, 160(34):223 – 238.

Jaupart, C. (1998). Gas loss from magmas through conduit walls during eruption. *Geological Society, London, Special Publications*, 145(1):73–90.

Jeffery, G. B. (1922). The motion of ellipsoidal particles immersed in a viscous fluid. *Proceedings of the Royal Society of London. Series A, Containing Papers of a Mathematical and Physical Character*, 102(715):161–179.

Jeffrey, D. J. and Acrivos, A. (1976). The rheological properties of suspensions of rigid particles. *AIChE Journal*, 22(3):417–432.

Johnston, D. M., Houghton, B., Neall, V., Ronan, K., and Paton, D. (2000). Impacts of the 1945 and 1995-1996 Ruapehu eruptions, New Zealand: An example of increasing societal vulnerability. *Geological Society of America Bulletin*, 112(5):720–726.

Kilgour, G., Blundy, J., Cashman, K., and Mader, H. M. (2013). Small volume andesite magmas and melt-mush interactions at Ruapehu, New Zealand: evidence from melt inclusions. *Contributions to Mineralogy and Petrology*, 1:1–22.

Kilgour, G., Manville, V., Pasqua, F. D., Graettinger, A., Hodgson, K., and Jolly, G. (2010). The 25 September 2007 eruption of Mount Ruapehu, New Zealand: Directed ballistics, surtseyan jets, and ice-slurry lahars. *Journal of Volcanology and Geothermal Research*, 191(12):1 – 14.

Kilgour, G., Saunders, K., Blundy, J., Cashman, K., Scott, B., Miller, C., and Mader, H. (2014). Timescales of magmatic processes at Ruapehu volcano from diffusion chronometry and their comparison to monitoring data. *JVGR*, 1:1–14.

Kress, V. and Carmichael, I. (1991). The compressibility of silicate liquids containing Fe_2O_3 and the effect of composition, temperature, oxygen fugacity and pressure on their redox states. *Contributions to Mineralogy and Petrology*, 108:82–92.

Lange, R. A. and Carmichael, I. S. (1987). Densities of Na_2O-K_2O-MgO-MgO-FeO-Fe_2O_3-Al_2O_3-TiO_2-SiO_2 liquids: New measurements and derived partial molar properties. *Geochimica et Cosmochimica Acta*, 51(11):2931 – 2946.

Lavallee, Y., Hess, K.-U., Cordonnier, B., and Bruce Dingwell, D. (2007). Non-Newtonian rheological law for highly crystalline dome lavas. *Geology*, 35(9):843–846.

Lejeune, A., Bottinga, Y., Trull, T., and Richet, P. (1999). Rheology of bubble-bearing magmas. *Earth and Planetary Science Letters*, 166(12):71 – 84.

Lejeune, A.-M. and Richet, P. (1995). Rheology of crystal-bearing silicate melts: An experimental study at high viscosities. *Journal of Geophysical Research: Solid Earth*, 100(B3):4215–4229.

Llewellin, E. and Manga, M. (2005). Bubble suspension rheology and implications for conduit flow. *Journal of Volcanology and Geothermal Research*, 143(1):205–217.

Llewellin, E. W., Mader, H. M., and Wilson, S. D. R. (2002a). The constitutive equation and flow dynamics of bubbly magmas. *Geophysical Research Letters*, 29(24):23–1–23–4.

Llewellin, E. W., Mader, H. M., and Wilson, S. D. R. (2002b). The rheology of a bubbly liquid. *Proceedings of the Royal Society of London. Series A: Mathematical, Physical and Engineering Sciences*, 458(2020):987–1016.

Mader, H., Llewellin, E., and Mueller, S. (2013). The rheology of two-phase magmas: A review and analysis. *Journal of Volcanology and Geothermal Research*, 257(0):135 – 158.

Manga, M., Castro, J., Cashman, K. V., and Loewenberg, M. (1998). Rheology of bubble-bearing magmas. *Journal of Volcanology and Geothermal Research*, 87(1):15–28.

Manga, M. and Loewenberg, M. (2001). Viscosity of magmas containing highly deformable bubbles. *Journal of Volcanology and Geothermal Research*, 105(1):19–24.

Marsh, B. (1988). Crystal size distribution (CSD) in rocks and the kinetics and dynamics of crystallization. *Contributions to Mineralogy and Petrology*, 99(3):277–291.

Melnik, O., Barmin, A., and Sparks, R. (2005). Dynamics of magma flow inside volcanic conduits with bubble overpressure buildup and gas loss through permeable magma. *Journal of Volcanology and Geothermal Research*, 143:53 – 68.

Moore, G. and Carmichael, I. S. E. (1998). The hydrous phase equilibria (to 3 kbar) of an andesite and basaltic andesite from western Mexico: constraints on water content and conditions of phenocryst growth. *Contributions to Mineralogy and Petrology*, 130:304–319.

Mueller, S., Llewellin, E. W., and Mader, H. M. (2010a). The rheology of suspensions of solid particles. *Proceedings of the Royal Society A: Mathematical, Physical and Engineering Science*, 466(2116):1201–1228.

Mueller, S., Llewellin, E. W., and Mader, H. M. (2011). The effect of particle shape on suspension viscosity and implications for magmatic flows. *Geophysical Research Letters*, 38(13):n/a–n/a.

Mueller, T., Watson, E. B., and Harrison, T. M. (2010b). Applications of diffusion data to high-temperature earth systems. *Reviews in Mineralogy and Geochemistry*, 72(1):997–1038.

Muir, D., Blundy, J., and Rust, A. (2012). Multiphase petrography of volcanic rocks using element maps: a method applied to Mount St. Helens, 1980-2005. *Bulletin of Volcanology*, 74(5):1101–1120.

Nakagawa, M., Wada, K., Thordarson, T., Wood, C. P., and Gamble, J. A. (1999). Petrologic investigations of the 1995 and 1996 eruptions of Ruapehu volcano, New Zealand: formation of discrete and small magma pockets and their intermittent discharge. *Bulletin of Volcanology*, 61:15–31.

Nakagawa, M., M., Wada, K., K., and Wood, C. P. (2002). Mixed magmas, mush chambers and eruption triggers: Evidence from zoned clinopyroxene phenocrysts in andesitic scoria from the 1995 eruptions of Ruapehu Volcano, New Zealand. *Journal of Petrology*, 43(12):2279–2303.

Nakamura, M. (1995). Continuous mixing of crystal mush and replenished magma in the ongoing Unzen eruption. *Geology*, 23(9):807–810.

Pal, R. (2003). Rheological behavior of bubble-bearing magmas. *Earth and Planetary Science Letters*, 207(1):165–179.

Papale, P., Moretti, R., and Barbato, D. (2006). The compositional dependence of the saturation surface of H_2O + CO_2 fluids in silicate melts. *Chemical Geology*, 229:78 – 95.

Picard, D., Arbaret, L., Pichavant, M., Champallier, R., and Launeau, P. (2011). Rheology and microstructure of experimentally deformed plagioclase suspensions. *Geology*, 39(8):747–750.

Picard, D., Arbaret, L., Pichavant, M., Champallier, R., and Launeau, P. (2013). The rheological transition in plagioclase-bearing magmas. *Journal of Geophysical Research: Solid Earth*, 1:1–15.

Pistone, M., Caricchi, L., Ulmer, P., Burlini, L., Ardia, P., Reusser, E., Marone, F., and Arbaret, L. (2012). Deformation experiments of bubble- and crystal-bearing magmas: Rheological and microstructural analysis. *Journal of Geophysical Research: Solid Earth*, 117(B5):B05208.

Pistone, M., Caricchi, L., Ulmer, P., Reusser, E., and Ardia, P. (2013). Rheology of volatile-bearing crystal mushes: Mobilization vs. viscous death. *Chemical Geology*, 345:16 – 39.

Price, R. C., Gamble, J. A., Smith, I. E. M., Maas, R., Waight, T., Stewart, R. B., and Woodhead, J. (2012). The anatomy of an andesite volcano: a time-stratigraphic study of andesite

petrogenesis and crustal evolution at Ruapehu Volcano, New Zealand. *Journal of Petrology*, 53(10):2139–2189.

Rust, A., Cashman, K., and Wallace, P. (2004). Magma degassing buffered by vapor flow through brecciated conduit margins. *Geology*, 32(4):349–352.

Rust, A. and Manga, M. (2002). Effects of bubble deformation on the viscosity of dilute suspensions. *Journal of non-newtonian fluid mechanics*, 104(1):53–63.

Saar, M. O., Manga, M., Cashman, K. V., and Fremouw, S. (2001). Numerical models of the onset of yield strength in crystal-melt suspensions. *Earth and Planetary Science Letters*, 187(34):367 – 379.

Sato, H. (2005). Viscosity measurement of subliquidus magmas:1707 basalt of Fuji volcano. *Journal of Mineralogical and Petrological Sciences*, 100(4):133–142.

Scott, B. (2013). A revised catalogue of Ruapehu volcano eruptive activity : 1830-2012. GNS Science Report 2013/45.

Shaw, H. R. (1972). Viscosities of magmatic silicate liquids; an empirical method of prediction. *American Journal of Science*, 272(9):870–893.

Shields, J. K., Mader, H. M., Pistone, M., Caricchi, L., Floess, D., and Putlitz, B. (2014). Strain-induced outgassing of three-phase magmas during simple shear. *Journal of Geophysical Research: Solid Earth*, 119(9):6936–6957.

Truby, J. M., Mueller, S. P., Llewellin, E. W., and Mader, H. M. (2014). The rheology of three-phase suspensions at low bubble capillary number. *Proceedings of the Royal Society of London A: Mathematical, Physical and Engineering Sciences*, 471(2173).

Villeneuve, N., Neuville, D. R., Boivin, P., Bachèlery, P., and Richet, P. (2008). Magma crystallization and viscosity: A study of molten basalts from the Piton de la Fournaise volcano (La Réunion island). *Chemical Geology*, 256(34):242 – 251. 8th Silicate Melt Workshop.

Vona, A., Romano, C., Dingwell, D., and Giordano, D. (2011). The rheology of crystal-bearing basaltic magmas from Stromboli and Etna. *Geochimica et Cosmochimica Acta*, 75(11):3214 – 3236.

Vona, A., Romano, C., Giordano, D., and Russell, J. (2013). The multiphase rheology of magmas from Monte Nuovo (Campi Flegrei, Italy). *Chemical Geology*, 346(0):213 – 227.

Wallace, P. J. (2005). Volatiles in subduction zone magmas: concentrations and fluxes based on melt inclusion and volcanic gas data. *Journal of Volcanology and Geothermal Research*, 140:217 – 240.

10. Figure and table captions

Table 1 Bulk composition of a representative Ruapehu scoria (sample number - 1977A). This starting composition was used for all rheological modelling. Volatiles (*) were determined from SIMS analysis (Kilgour et al., 2013)

Table 2 Representative crystallinity (Kilgour et al., 2013) and vesicularity (GNS Science, unpublished data) of Ruapehu scoria. Microlite content and mean aspect ratios (length:width) were determined in this study. Vesicularity values were determined from thin section point counts (*) or by the Archimedes method (†)(Houghton and Wilson, 1989)

Table 3 Average major element composition of groundmass glass from historical Ruapehu eruptions from Kilgour et al. (2013). H_2O values are the maximum obtained from melt inclusion analyses, after Kilgour et al. (2013). Standard deviations are given in parentheses.

Fig. 1 Theoretical model set-up of calculations. The decrease in temperature and pressure is not to scale, but shows the main changes that will lead to rheological changes with decreasing temperature and pressure.

Fig. 2 A comparison between melt fraction as a function of temperature determined experimentally (at $\sim$ 100 MPa and H_2O-saturated conditions) against the thermodynamic model (MELTS). Our experimental data along with that of (Blatter and Carmichael, 1998) compare favourably to MELTS (Ghiorso and Sack, 1995; Asimow and Ghiorso, 1998). This gives us confidence in the model outputs for the subsequent chemical and rheological calculations.

Fig. 3 An example of a microlite-bearing groundmass glass from the 1996 eruption of Ruapehu. We obtained SEM-derived X-ray element maps of the groundmass (a), which we in turn converted to binary images of Al (b) and Mg (c) with image analysis software. We then extracted the abundance of plagioclase (b) and pyroxene (c) crystals from the groundmass using

image analysis software (*ImageJ*). The area and volume fraction of plagioclase and pyroxene microlites were then calculated. The scale bar in all images is 25 μm.

Fig. 4 (a) Profile of the microlite growth curves used in the model. Nucleation occurs rapidly at the onset of decompression, trending towards the final microlite content. For this model, we assume isothermal conditions. Relative viscosities due to microlite growth for the 977 °C (b) and 1030 °C (c) magmas are also shown at a range of strain rates ($\dot{\gamma}$).

Fig. 5 Back scattered electron images of three representative scoria from Ruapehu. These images illustrate the vesicle, phenocryst, and microlite textures in scoria from 1969, 1977, and 1995. Plagioclase (pl), pyroxene (py), and glass (gl) are highlighted. Note the difference in vesicularity and microlite content. The scale bar in each image is 100 μm in all images.

Fig. 6 Variations in melt composition and melt viscosity ($\log\mu$) with pressure and composition. The thermodynamic model MELTS (Ghiorso and Sack, 1995; Asimow and Ghiorso, 1998) enabled us to calculate equilibrium crystallisation conditions from the same bulk rock composition and also determine the melt composition. At each step, we calculated the melt viscosity using Giordano et al. (2008).

Fig. 7 Bubble volume fraction (ϕ_b) as a function of pressure calculated using the solubility model of Papale et al. (2006) and assuming an ideal gas mixture. Due to the similarity between the 1969, 1977 and 1996 magmas, the curves are almost identical. For clarity, only the 977 °C and 2 wt % H_2O magma is plotted on this diagram. Here we compare Ruapehu magmas that are volatile-poor (i.e., 2 wt % H_2O and 1000 ppm CO_2; Kilgour et al., 2013) with magmas of the same composition and CO_2 content, but with 3, 4, and 5 wt % H_2O.

Fig. 8 Measured clast vesicularity (bulk bubble volume fraction) from the June-July, 1996 eruption of Ruapehu from a proximal source to the vent. Upper, middle and lower refer to the stratigraphic position of the identified subunits. Black diamonds represent average values within the range (minimum and maximum). The vertical dashed line is at the overall average of 55 % - the approximate bubble volume fraction determined from the modelling (Fig. 7). These are unpublished data from GNS Science courtesy of M. Rosenberg *pers. comm.*

Fig. 9 The effect of bubble growth on the magma volume (for 100 g of magma) as a function of pressure. The gas volume was calculated using the solubility model of Papale et al. (2006) and assuming an ideal gas mixture.

Fig. 10 Relative viscosity (η_b) of Ruapehu magma due to bubble growth. All three model magmas have very similar bubble volume fraction and consequently, the η_b due to bubbles is almost identical. For clarity, only results for the 977 °C magma are shown. ϕ_b refers to the bubble volume fraction, while upper ($\eta_{b,o}$) and lower ($\eta_{b,\infty}$) refer to the bounding relative viscosities. The upper boundary assumes that all bubbles are spherical (low Capillary number) and the lower boundary assumes elongated bubbles (high Capillary number). We ignore the effect of flow, i.e., $\dot{\gamma} = 0$.

Fig. 11 Newtonian melt viscosity ($\log\mu$) and apparent viscosity ($\log\eta_{cr}$) of Ruapehu magmas due to the addition of microlites and phenocrysts. Here, μ and η are in Pa s. (a) The 915 °C magma is microlite-free and contains a phenocryst volume fraction of ~ 0.3. With the addition of microlites for the 977 °C magma (b) and and the 1030 °C magma (c), the suspension viscosity increases significantly. For these calculations, we assumed a constant strain rate ($\dot{\gamma}$) of 1 s^{-1}. Note that in the modelling (see text), we calculate the melt + phenocrysts and then add microlites.

Fig. 12 Three-phase apparent viscosity of Ruapehu magmas. This plot shows the combined effect of crystals (microlites and phenocrysts) and bubbles on the apparent magma viscosity ($\log\,\eta$), where η is in Pa s. The effect of bubbles is assumed to have a high capillary number, i.e., bubbles are considered to have become elongated due to high shear stress within the upper conduit leading to a reduction of apparent viscosity.

Table 1: Bulk composition of a representative Ruapehu scoria (sample number - 1977A). This starting composition was used for all rheological modelling. Volatiles (*) were determined from SIMS analysis (Kilgour et al., 2013)

Eruption year	1977
Sample number	1977A
Major elements	(wt %)
SiO_2	60.44
Al_2O_3	16.43
Fe_2O_3	7.65
MnO	0.07
MgO	3.62
CaO	7.08
Na_2O	2.55
K_2O	1.39
TiO_2	0.66
P_2O_5	0.14
H_2O*	2.00
CO_2*	0.01

Table 2: Representative crystallinity (Kilgour et al., 2013) and vesicularity (GNS Science, unpublished data) of Ruapehu scoria. Microlite content and mean aspect ratios (length:width) were determined in this study. Vesicularity values were determined from thin section point counts (*) or by the Archimedes method (†)(Houghton and Wilson, 1989)

Eruption date	1969	1977	1995	Aspect ratio
Total phenocryst (%)	29	31	26	
Total groundmass (%)	71	69	74	
Microlite (vol%)	0	30	20	
Mean clast vesicularity (%)	42*	20*	55†	
Phenocrysts				
Plagioclase	20	22	18	5:1
Clinopyroxene	4	4	3	2:1
Orthopyroxene	5	4	5	2:1

Table 3: Average major element composition of groundmass glass from historical Ruapehu eruptions from Kilgour et al. (2013). H_2O values are the maximum obtained from melt inclusion analyses, after Kilgour et al. (2013). Standard deviations are given in parentheses.

	Eruption date					
Major Element (wt %)	1969	[915 °C]	1977	[977 °C]	1995	[1030 °C]
SiO_2	72.07	(1.24)	67.93	(1.07)	63.20	(1.24)
Al_2O_3	13.32	(0.91)	13.95	(0.43)	15.34	(0.59)
FeO	3.20	(0.52)	6.07	(0.39)	6.47	(0.55)
MnO	0.05	(0.02)	0.09	(0.02)	0.11	(0.04)
MgO	0.49	(0.32)	1.22	(0.17)	2.50	(0.61)
CaO	2.06	(0.51)	3.90	(0.30)	5.58	(0.60)
Na_2O	3.83	(0.31)	2.33	(0.67)	3.18	(0.61)
K_2O	4.15	(0.30)	3.05	(0.16)	2.45	(0.26)
TiO_2	0.68	(0.08)	1.19	(0.05)	0.99	(0.08)
P_2O_5	0.13	(0.05)	0.25	(0.04)	0.17	(0.08)
H_20	2.00		2.00		2.00	
n	36		31		28	

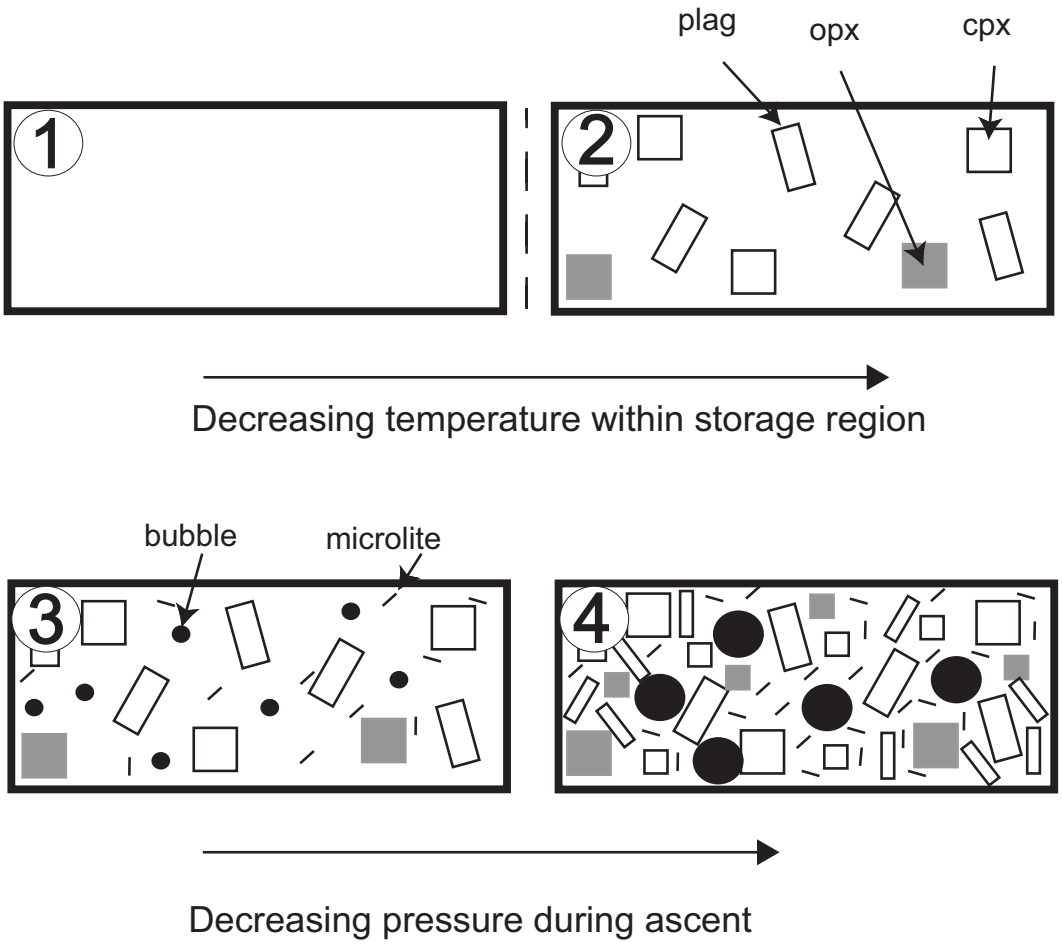

Figure 1: Theoretical model set-up of calculations. (1) The liquidus for this magma is 1150 °C, which means that above this temperature, the rheology of the magma is largely constrained by the bulk composition, H_2O content and temperature using the viscosity model of Giordano et al. (2008). (2) Isobaric cooling of the magma to its final eruption temperature (915, 977, and 1030 °C), allows plagioclase (plag), clinopyroxene (cpx), and orthopyroxene (opx) to crystallise. Without gas exsolution, the rheology of the magma is a crystal-melt, two-phase suspension. (3) Adiabatic decompression results in gas exsolution and bubble growth along with microlite formation. (4) Continued adiabatic decompression causes further bubble expansion and microlite growth. During bubble and microlite growth, we model the three-phase rheology of the system using the constitutive two-phase equations of Mader et al. (2013).

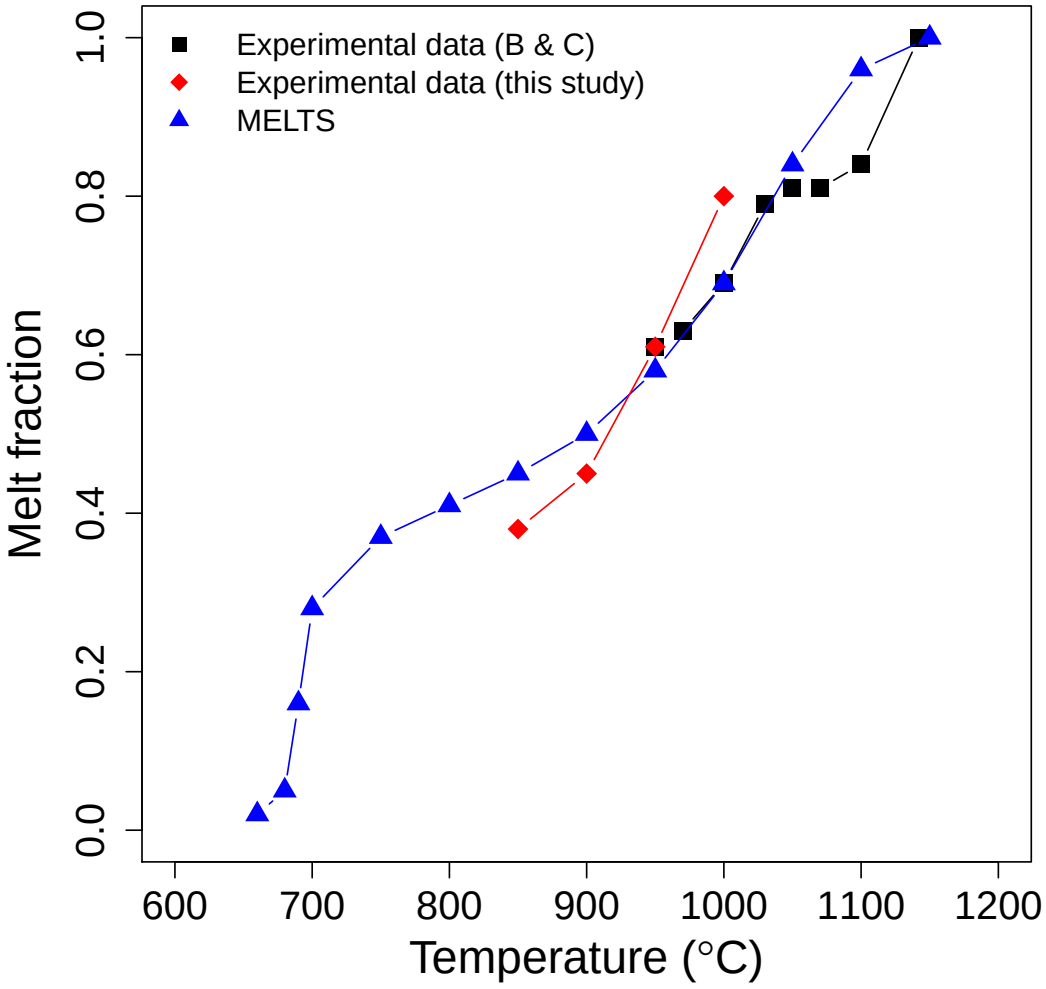

Figure 2: A comparison between melt fraction as a function of temperature determined experimentally (at $\sim$ 100 MPa and H$-$2O-saturated conditions) against the thermodynamic model (MELTS). Our experimental data along with that of (Blatter and Carmichael, 1998) (B & C) compare favourably to MELTS (Ghiorso and Sack, 1995; Asimow and Ghiorso, 1998). This gives us confidence in the model outputs for the subsequent chemical and rheological calculations.

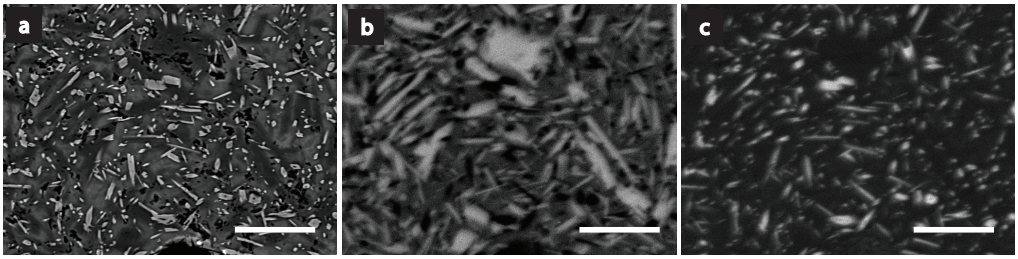

Figure 3: An example of a microlite-bearing groundmass glass from the 1996 eruption of Ruapehu. We obtained SEM-derived X-ray element maps of the groundmass (a), which we in turn converted to binary images of Al (b) and Mg (c) with image analysis software. We then extracted the abundance of plagioclase (b) and pyroxene (c) crystals from the groundmass using image analysis software (*ImageJ*). The area and volume fraction of plagioclase and pyroxene microlites were then calculated. The scale bar in all images is 25 μm.

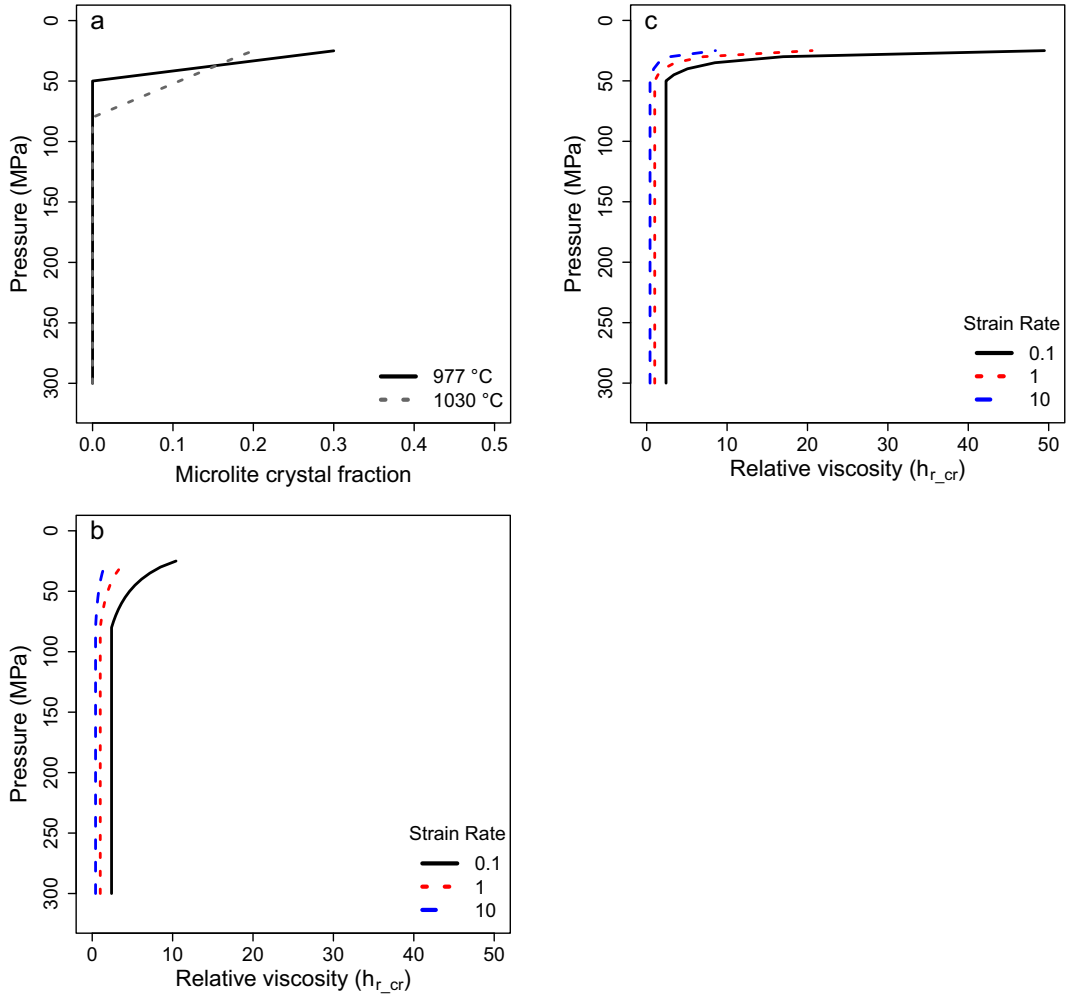

Figure 4: (a) Profile of the microlite growth curves used in the model. Nucleation occurs rapidly at the onset of decompression, trending towards the final microlite content. Here, the microlite crystal fraction is relative to the total volume. For this model, we assume isothermal conditions. Relative viscosities due to microlite growth for the 977 °C (b) and 1030 °C (c) magmas are also shown at a range of strain rates ($\dot{\gamma}$).

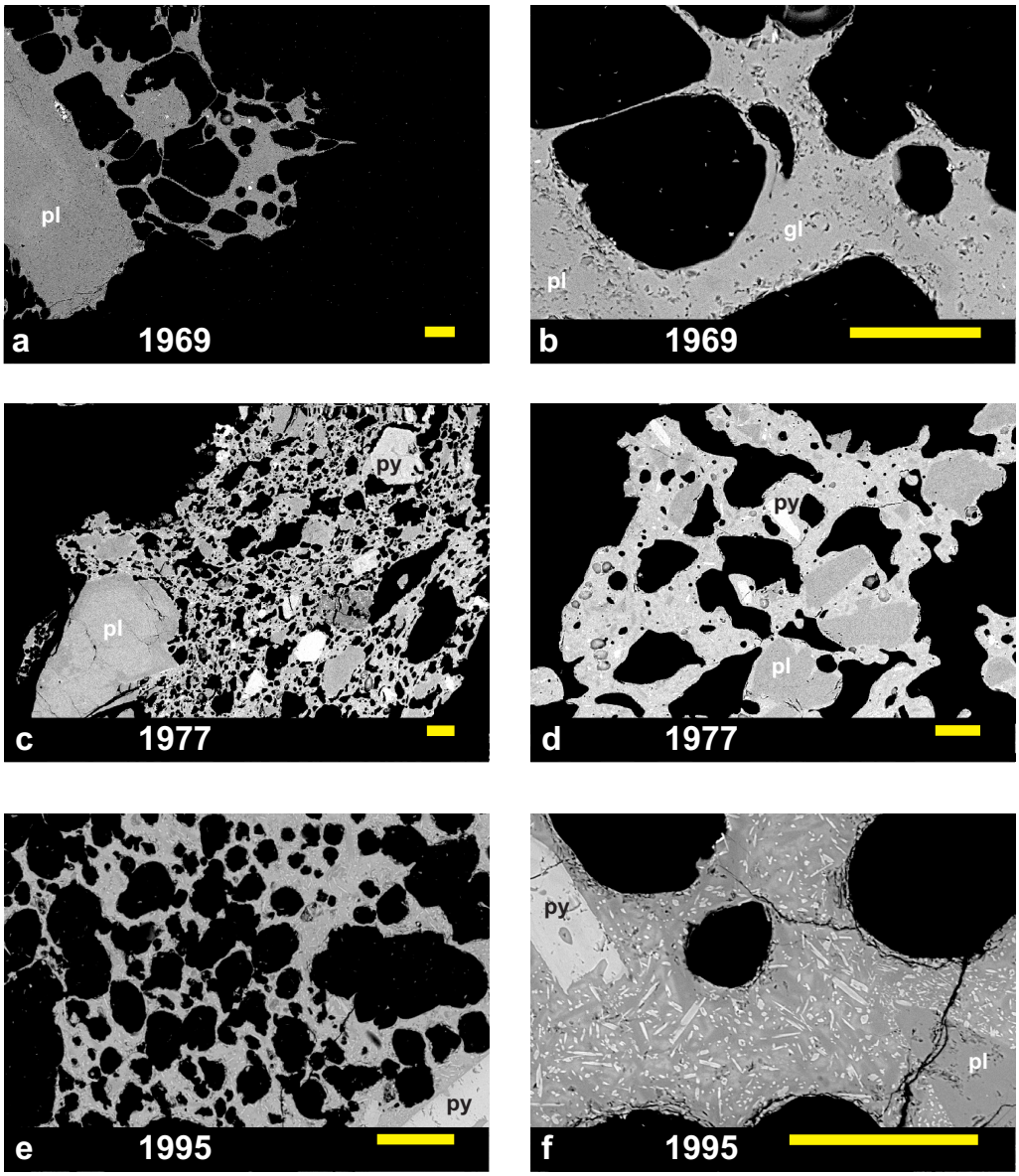

Figure 5: Back scattered electron images of three representative scoria from Ruapehu. These images illustrate the vesicle, phenocryst, and microlite textures in scoria from 1969, 1977, and 1995. Plagioclase (pl), pyroxene (py), and glass (gl) are highlighted. Note the difference in vesicularity and microlite content. The scale bar in each image is 100 μm.

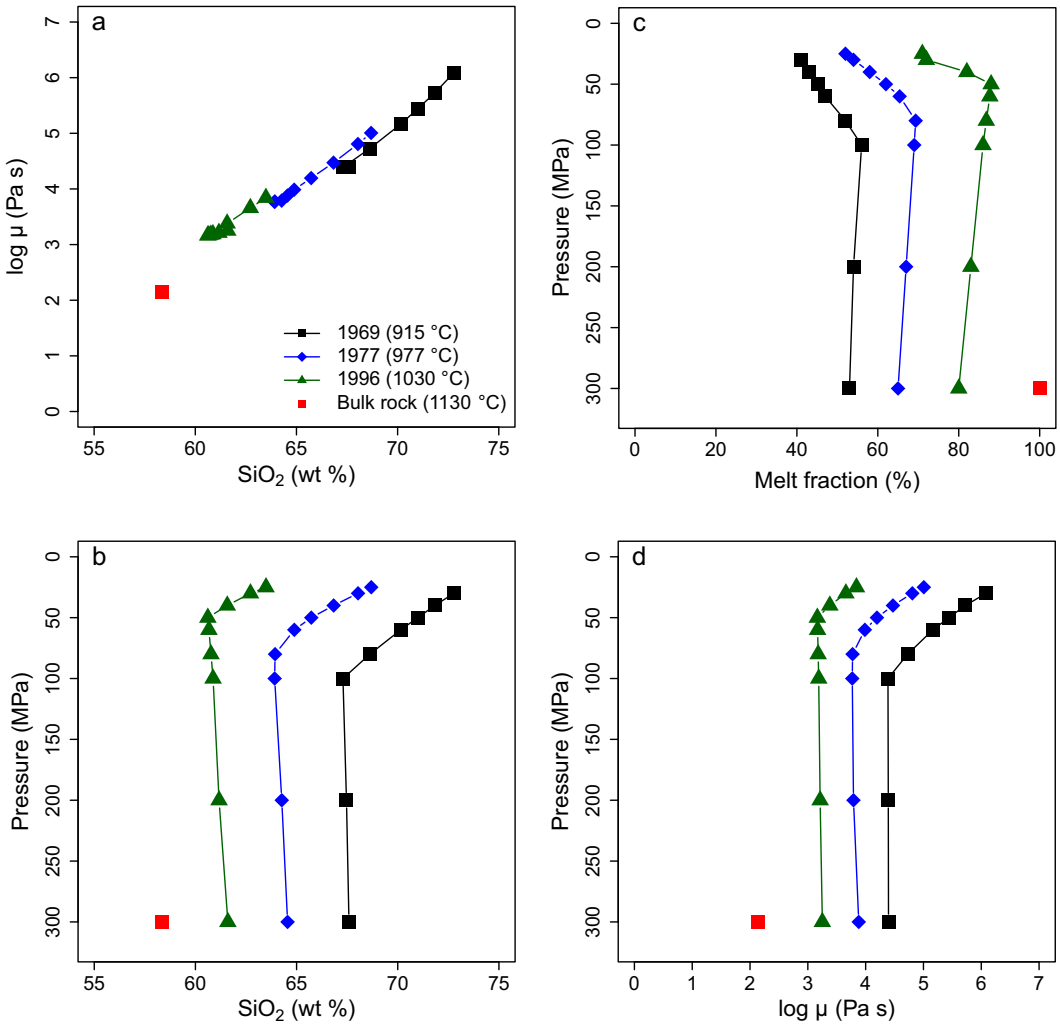

Figure 6: Variations in melt composition and melt viscosity (logμ) with pressure and composition. The thermodynamic model MELTS (Ghiorso and Sack, 1995; Asimow and Ghiorso, 1998) enabled us to calculate equilibrium crystallisation conditions from the same bulk rock composition and also determine the melt composition and melt fraction (relative to the total volume). At each step, we calculated the melt viscosity using Giordano et al. (2008).

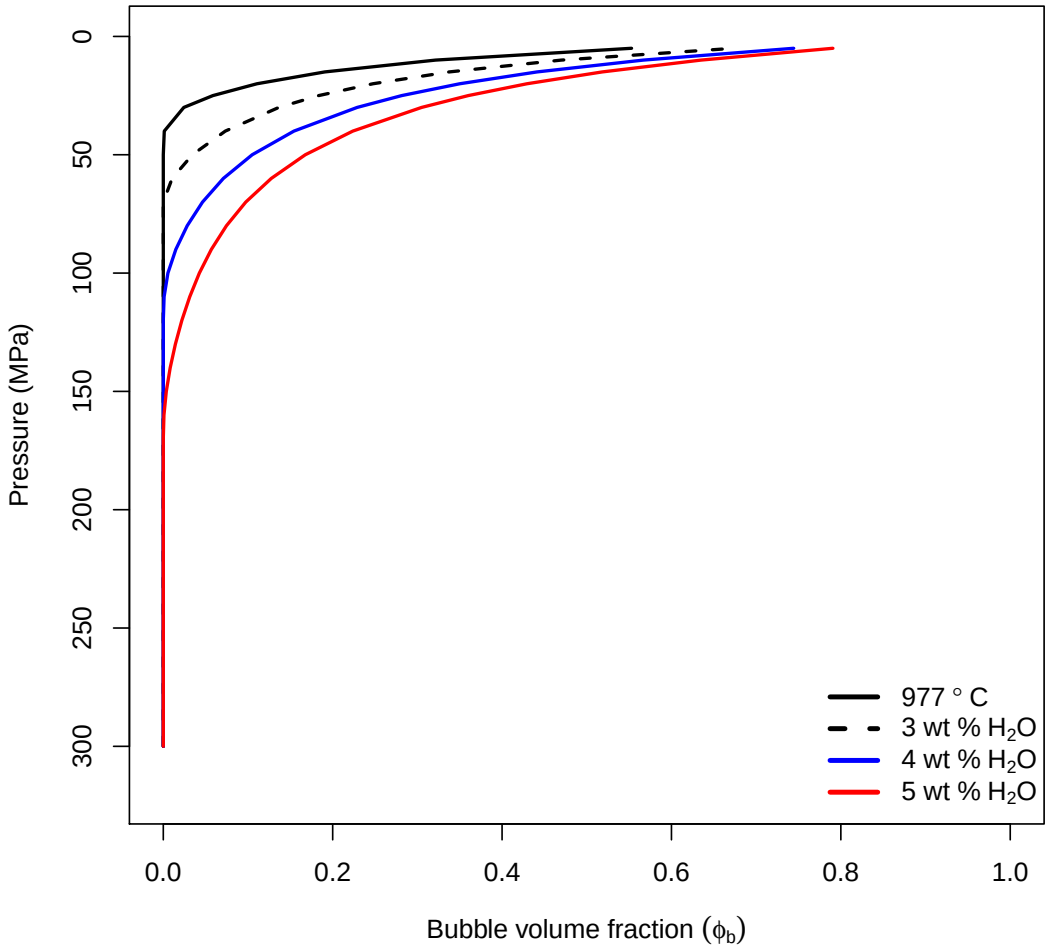

Figure 7: Bubble volume fraction (ϕ_b) as a function of pressure calculated using the solubility model of Papale et al. (2006) and assuming an ideal gas mixture. Due to the similarity between the 1969, 1977 and 1996 magmas, the curves are almost identical. For clarity, only the 977 °C and 2 wt % H_2O magma is plotted on this diagram. Here we compare Ruapehu magmas that are volatile-poor (i.e., 2 wt % H_2O and 1000 ppm CO_2; Kilgour et al., 2013) with magmas of the same composition and CO_2 content, but with 3, 4, and 5 wt % H_2O.

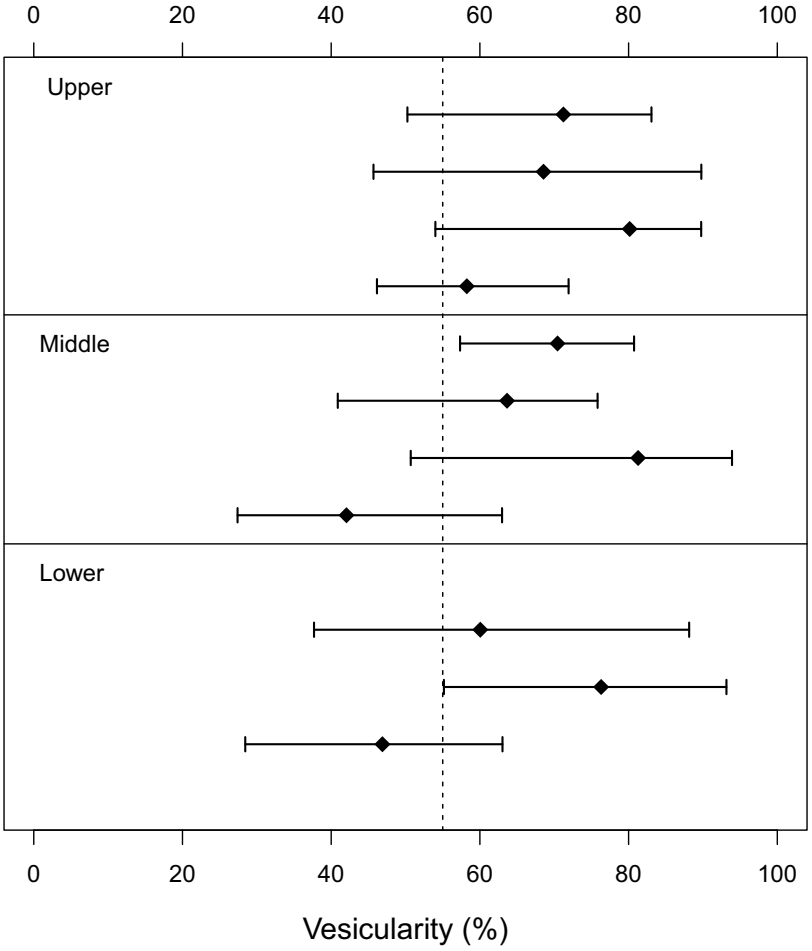

Figure 8: Measured clast vesicularity (phenocryst-free) from the June-July, 1996 eruption of Ruapehu from a proximal source to the vent. Upper, middle and lower refer to the stratigraphic position of the identified subunits. Black diamonds represent average values within the range (minimum and maximum). The vertical dashed line represents the bubble volume fraction at $\sim$ 5 MPa ($\sim$ 55 %) determined from the solubility modelling (Fig. 7). These are unpublished data from GNS Science courtesy of M. Rosenberg and B. Houghton *pers. comm.*

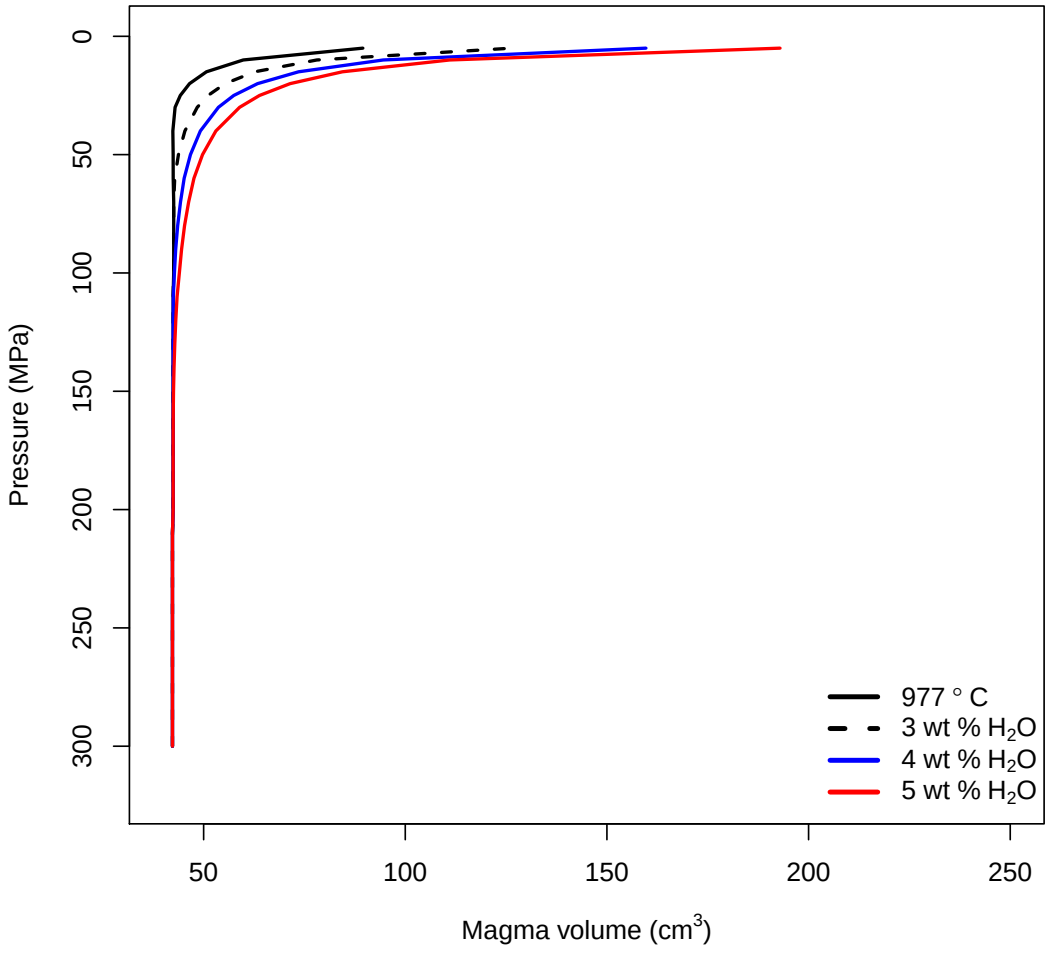

Figure 9: The effect of bubble growth on the magma volume (for 100 g of magma) as a function of pressure. The gas volume was calculated using the solubility model of Papale et al. (2006) and assuming an ideal gas mixture.

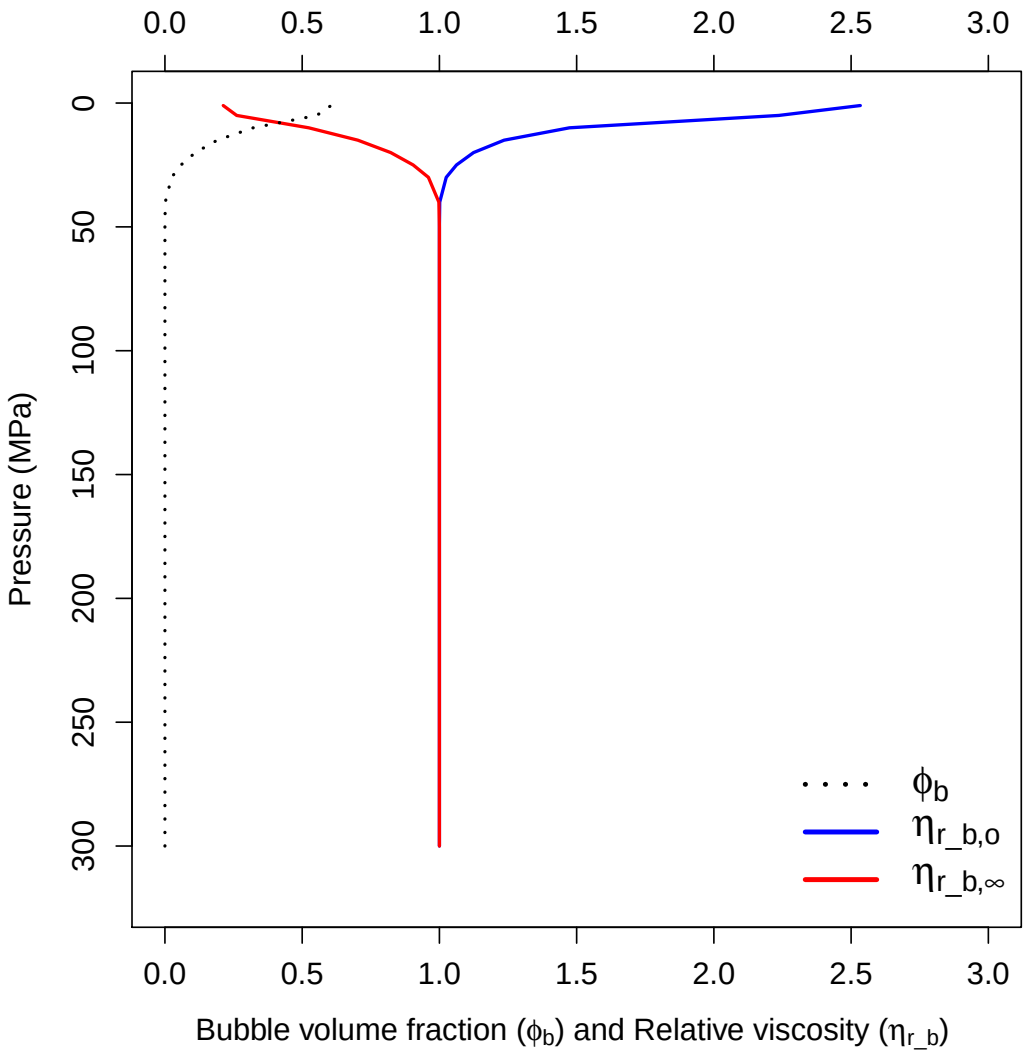

Figure 10: Relative viscosity (η_r_b) of Ruapehu magma due to bubble growth. All three model magmas have very similar bubble volume fraction and consequently, the η_r_b due to bubbles is almost identical. For clarity, only results for the 977 °C magma are shown. ϕ_b refers to the bubble volume fraction, while upper ($\eta_{r\_b,o}$) and lower ($\eta_{r\_b,\infty}$) refer to the bounding relative viscosities. The upper boundary assumes that all bubbles are spherical (low Capillary number) and the lower boundary assumes elongated bubbles (high Capillary number). We ignore the effect of flow, i.e., $\dot{\gamma} = 0$.

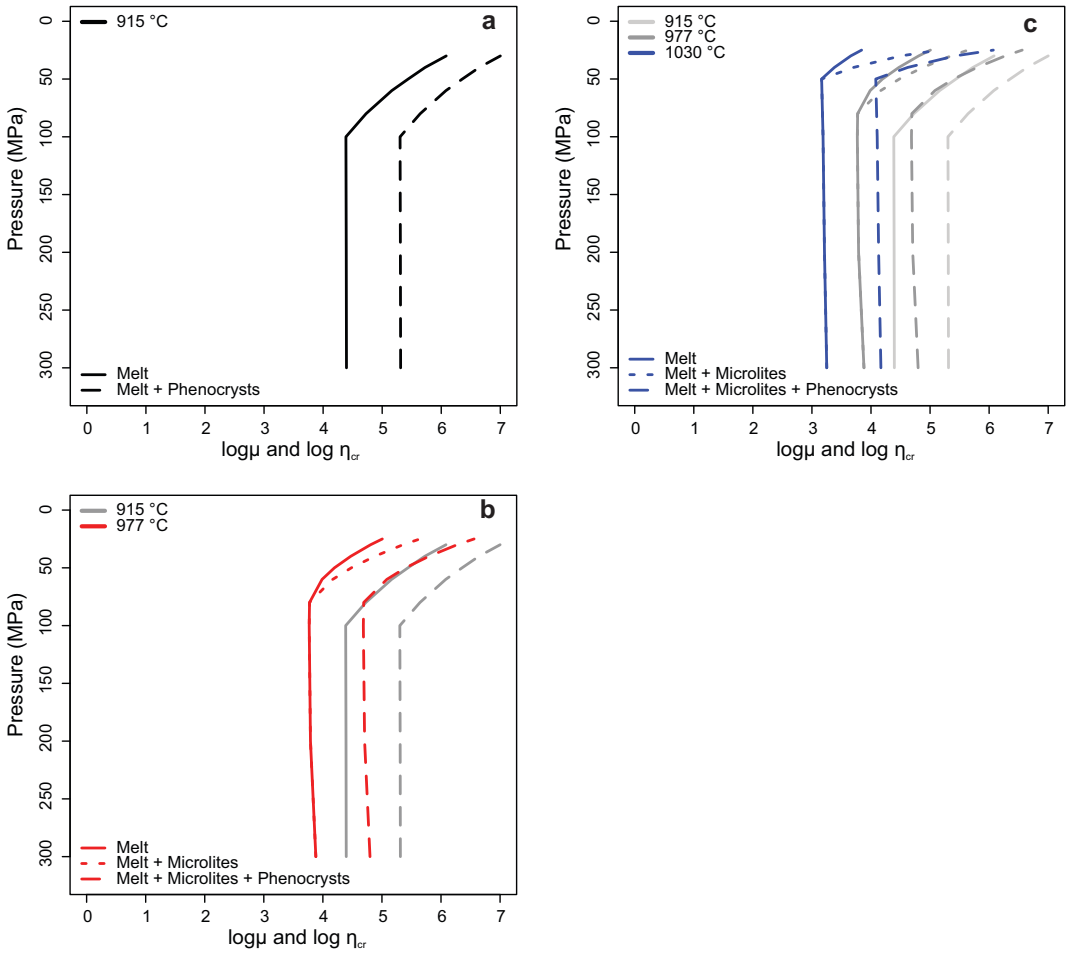

Figure 11: Newtonian melt viscosity ($\log\mu$) and apparent viscosity ($\log\eta_{cr}$) of Ruapehu magmas due to the addition of microlites and phenocrysts. Here, μ and η are in Pa s. (a) The 915 °C magma is microlite-free and contains a phenocryst volume fraction of ~ 0.3. With the addition of microlites for the 977 °C magma (b) and and the 1030 °C magma (c), the suspension viscosity increases significantly. For these calculations, we assumed a constant strain rate ($\dot{\gamma}$) of 1 s^{-1}. Note that in the modelling (see text), we calculate the melt + phenocrysts and then add microlites.

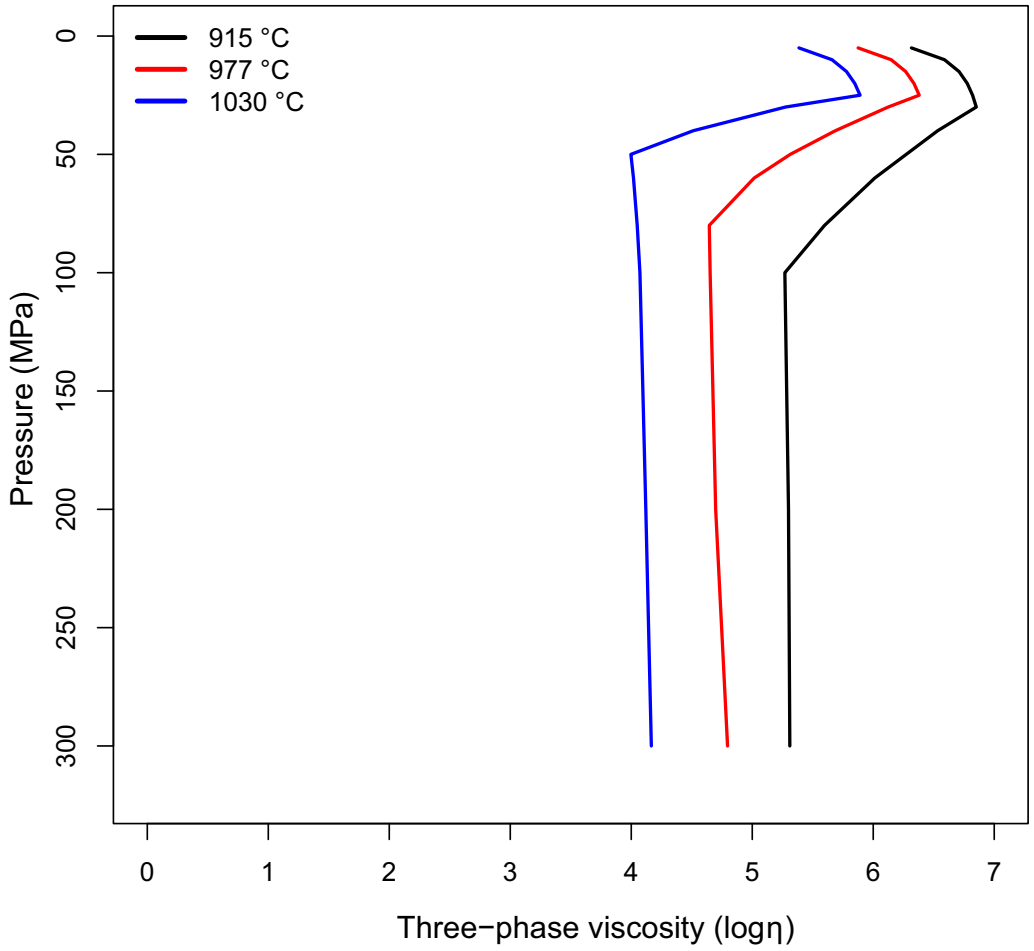

Figure 12: Three-phase apparent viscosity of Ruapehu magmas. This plot shows the combined effect of crystals (microlites and phenocrysts) and bubbles on the apparent magma viscosity (log η), where η is in Pa s. The effect of bubbles is assumed to have a high capillary number, i.e., bubbles are considered to have become elongated due to high shear stress within the upper conduit leading to a reduction of apparent viscosity.